Eng. Sci., 2022, **20**, 47–79

Engineered Science

DOI: https://dx.doi.org/10.30919/es8d737

Progress in Catalysis for Industrial Applications

Cedric Karel Fonzeu Monguen,[1, 2,†] Samuel Daniel,[1, 2,†] Dan Yu,[1] Olumide Bolarinwa Ayodele,[1] Zhen-Yu Tian[1, 2,*]

Abstract

Catalysis is the process of enhancing the rate of transformation of chemical compounds into other products on selective catalysts. It is a fascinating technique utilized in the environmental and petrochemical industries. This review summarized the current progress in the oxidation of Volatile organic substances (VOCs), NO_x reduction, dry and steam methane reforming, and the Fischer-Tropsch synthesis (FTs). The catalysts' preparation techniques, characterizations and reaction mechanisms were underlined. This work identified primary causes of catalytic deactivation, such as carbon deposition, sulphur/alkali poisoning, adverse water effects and ways to improve catalytic performance in the phase of such negative effects. Over the past four years, publications on catalysis were found to be approximately 63%, 24%, 7%, and 26% for VOCs oxidation, NOx selective conversion, FTs, and methane reforming, respectively. Finally, future perspectives were highlighted, such as the doping of a catalyst with N, Br, and Si, to improve catalyst performance and the designing of characterization techniques such as Helium ion microscopy, Raman spectroscopy, and Electron energy loss spectroscopy to study the detailed properties of the catalyst. More research on developing a new catalyst to convert low-priced chemicals into high-demand chemical products, alkane to alkene, at low temperatures were also covered.

Keywords: Catalysis; Complete abatement; Dry and steam reforming; Fischer-Tropsch synthesis; Selective conversion.
Received: 10 May 2022; Revised: 07 June 2022; Accepted: 08 June 2022.
Article type: Review article.

1. Introduction

Catalysis is the process of enhancing the rate of chemical reaction that involves converting certain chemical compounds into other forms of products on selective catalysts. Catalysis is applied in various environmental and petrochemical fields, such as the oxidation of volatile organic compounds (VOCs), NO_x reduction, methane reforming, and Fischer-Tropsch synthesis (FTs).

Catalysis in VOCs requires lower temperatures (around 150-500 °C) than conventional thermal oxidation processes (generally operate at 650-1100 °C).[1] Thus, fewer energy requirements and formation of negligible or non-amount of NO_x in the combustion chamber. Hence, it would be considered an eco-friendly and cost-effective technology.[2] The complete catalytic oxidation of VOCs to carbon dioxide and water has been considered one of the most effective methods to abate VOCs to low concentrations and meet strict environmental regulations.[3,4]

Several catalysts have been used for catalysis in VOCs oxidation, selective conversion, FT synthesis methane reforming. The commonly utilized catalysts are noble metals (Pt, Rh, Au, Pd, and Ag),[3-5-7] transition metal oxides (Ni, Cu, Co, Cr, Mn, Mo, V, Zn, Zr, Ce, Ti, and Fe) and their mixtures (*e.g.*, MnO_x-CuO_x and MnO_x-CeO_2),[8,12] perovskites,[13,16] zeolites,[17,19] single-atom catalyst,[20,24] as shown in Fig. 1.

Over the years, efforts have been made in catalysis by improving the catalytic properties of such catalysts through stability improvement. For example, Ru substituted in $LaAlO_3$ offers good thermal stability due to the strong interaction between Ru and Al during FTs.[25,28] In terms of catalyst doping.[28,29] the incorporation of Ni into $MgAl_2O_4$ spinel catalysts exhibited good catalytic performance towards dry reforming of CH_4 with CO_2 due to the presence of oxygen vacancy created by Ni in the spinel structure by the lattice distortion effect. Carabineiro *et al.*[2] doped Ce with Ln and Cu, and found that the following activity order for the Cu-free samples, regarding ethyl acetate (EtOAc) conversion, that CeO_2 >> $Ce_{0.5}Pr_{0.5}O_{1.75}$ > $Ce_{0.5}Sm_{0.5}O_{1.75}$ > $Ce_{0.5}Gd_{0.5}O_{1.75}$ > $Ce_{0.5}Nd_{0.5}O_{1.75}$ > $Ce_{0.5}La_{0.5}O_{1.75}$, showing the adverse effect of lanthanide-doping. Cu incorporation into the Ce and Ln oxides enhanced the catalyst's performance without affecting the activity. Moreover, the performance was asserted to be

[1] *Institute of Engineering Thermophysics, Chinese Academy of Sciences, Beijing 100190, China.*
[2] *University of Chinese Academy of Sciences, Beijing 100049, China.*
[†] *Both contributed equally.*
**Email:* tianzhenyu@iet.cn (Z-Y Tian)

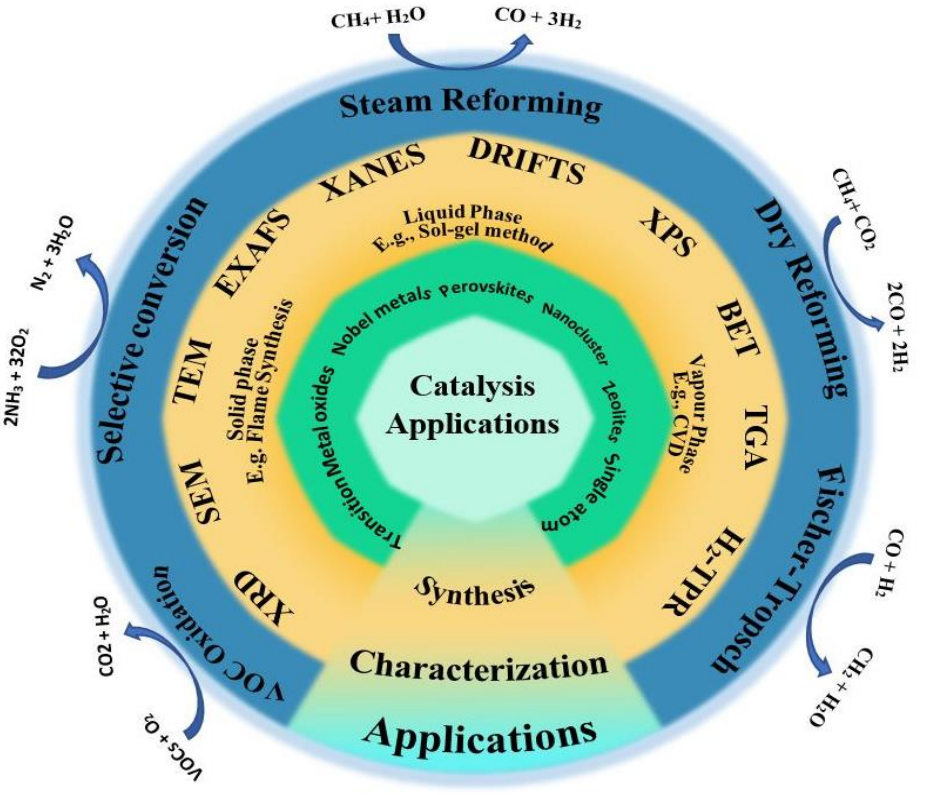

Fig. 1 Illustration of an overview of catalysis, including different types of catalysts, their synthesis methods, and applications.

Cu/CeO_2 and $Cu/Ce_{0.5}Pr_{0.5}O_{1.75}$, and both samples presented complete EtOAc conversion at ≈290 °C.

To study the loading effect for improving catalytic activity,[30,33] Tian's group introduced Mn into Co_3O_4 and then introduced Cu using a PSE-CVD synthesis technique to control VOCs efficiently. The results show a great activity toward a complete reduction of C_2H_2 and C_3H_6 at low temperatures, and no CO was formed during the oxidation process. The result confirmed that the copper-based ceria catalyst was highly active at 240 °C for the dehydrogenation reaction, with 93% conversion and 98% selectivity.[34] Ayodele *et al.* have found nanocluster PtCu as a promising catalyst for C_2H_2 conversion into C_2H_4; the allowing of Pt with Cu was responsible for the high selectivity of C_2H_4 (~ 98%).[35] Regarding the effect of loading ratio during dry reforming of methane, Ni loading for the methane dry reforming over $Ni/Ce_{0.62}Zr_{0.38}O_2$ catalysts prepared via incipient wetness impregnation with various loadings of nickel (2, 4, and 10 wt%.) was found to exhibit high performance toward conversions of CO_2 and CH_4 with an optimum ratio H_2/CO = 1 from the catalysts with the 10 wt%. Ni content.[36]

Catalysis covers several areas of industrial applications like dehydrogenation of alkane to alkene, complete combustion of VOCs, NOx reduction, FTs (conversion of mixture CO and H_2 into liquid hydrocarbon), and methane reforming (method of producing syngas through the reaction of CH_4 and CO_2).

Despite much interest in catalysis, only limited reviews summarized what had been done so far in this field. Moreover, most studies focused on either reviewing catalytic oxidation,[37] selective catalytic reduction,[38] reforming,[39] or FTs.[40] To the best of our knowledge, there have been scarce literature reviews that comprehensively discuss all the aspects of catalysis. This review largely focused on the general overview of catalysis, catalyst characterization, and its application on complete abatement of VOCs, NO_x selective conversion, FTs, and methane reforming. Catalytic deactivation by water, sulfur poisoning, alkali poisoning, and the strategies to overcome the shortcoming was discussed. Also, the kinetic mechanism for the oxidation of VOCs, selective catalytic reduction of NOx, reforming, and FTs synthesis was explored.

2. Catalyst preparation techniques

Practically all approaches involving chemical and physical transformations can be employed to prepare catalysts in catalysis. The techniques were divided into three categories: solid, liquid, and vapor-phase. The solid-phase preparation techniques include high temperature, flux growth, combustion, nitrate decomposition, MOF-derived (MOFs: Metal-organic frameworks), and pulsed laser methods. The liquid-phase preparation techniques involve sol-gel, hydrothermal, precipitation, micro-emulsion, microwave, electro-chemical, and high-temperature techniques. The vapor-phase preparation techniques consist of flame spray pyrolysis (FSP), pulse spray evaporation-chemical vapor deposition (PSE-CVD), atomic layer deposition (ALD), magnetron sputtering, and plasma methods. Fig.2 presents the pictorial representation of the regrouped techniques.

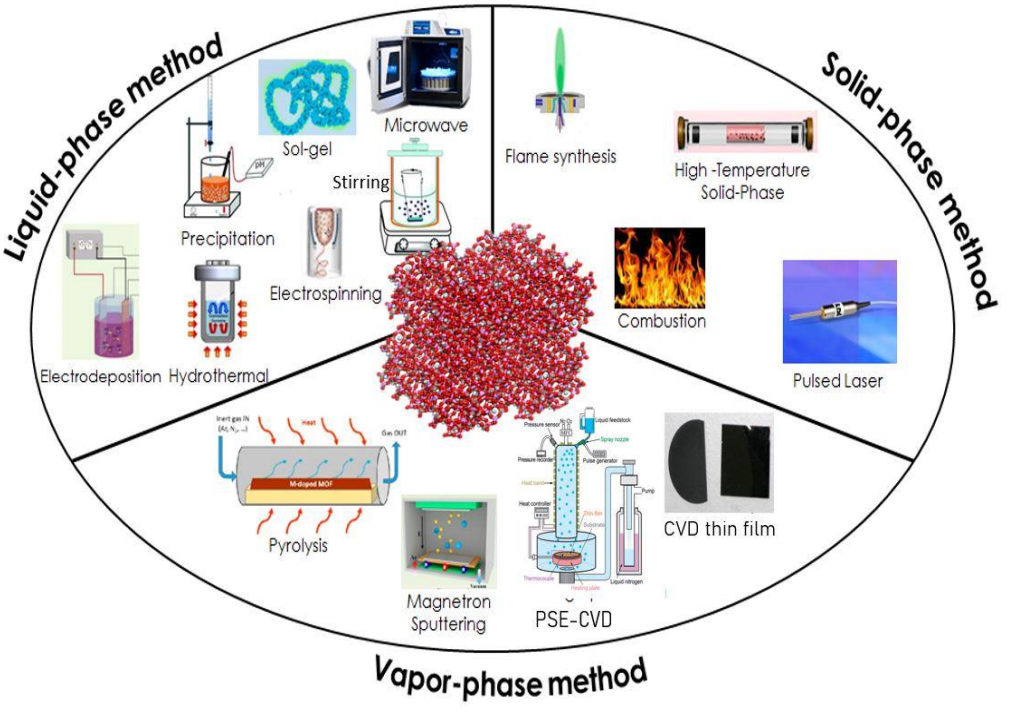

Fig. 2 Different catalysts synthesis methods for preparation in catalysis.

2.1.1 Liquid-phase method

2.1.1.1 Impregnation

Impregnation is a simple method of synthesizing a catalyst. This process involves the use of a certain volume of solution containing active metal precursors, mixed with catalyst support, and adsorbed the active metal onto the support through an ion-exchange/adsorption process. This method is attractive because of its technical simplicity, low costs, and few numbers of waste. Several nano-catalysts have been prepared for different applications such as: Pd/TiO_x,[41] $Ce_{0.5}LnO$ and $Cu/Ce_{0.5}Ln_{0.5}O_{1.75}$,[2] CoO/NC (nanocrystals),[42] Co_2SiO_4 and Co_3O_4,[43] $Fe\text{-}SiO_2$,[44] Ru/CNT (carbon nanotube),[45] Co/SiO_2,[46] γ -Al_2O_3,[47] $Pt1@CeO_2$ (single atom),[20] $Ni/MgO\ Al_2O_3$,[48] $CeO_2\text{-}ZnAl_2O_4$[49] Ni-Ru,[50] Ni/La_2O_3,[51] Co_2Ni/CeO_2,[52] $Ni@Al_2O_3/AlN$,[53] $La_2O_2CO_3$-modified Ni/Al_2O_3,[54] Ag promoted Co/Al_2O_3,[55] N-GNS (Graphene Nanosheets) supported Co,[56] $Ni\text{-}Si/ZrO_2$,[57] Cu,[58] CuO/CeO_2,[59] Ag/SBA-15[60] (SBA: Santa barbara amorphous), Co_3O_4/Al_2O_3[61] and Cu/CeO_2.[62]

2.1.1.2 Precipitation/ Co-precipitation

Precipitation or co-precipitation is a traditional and widely used technique to prepare a nanoparticle as bulk or supported catalysts. This method combined aqueous phase metal salts and alkali solutions to produce an insoluble metal hydroxide. Metal hydroxides are precipitated from their precursor salt solution due to their low solubility. The coprecipitated catalyst undergoes washing, filtering, and drying, then calcined in a furnace. Co-precipitation can be used for simultaneous precipitation of more than one component. The main advantage of this process is to create a pure and homogeneous catalyst. Moreover, we can get nanoparticles, and single-atom catalysts using this technique for catalysis, such as $Ce_{0.5}Zr_{0.5}O_2$,[63] $CexZr_{1x}O_2$,[64] Fe_5C_2 and Si/Ti,[65] Ni/MgO (single atom),[66] $Ni1/CeO_2$,[12] Sandwiched $SiO_2@Ni@ZrO_2$,[67] $CeO_2/ZnAl_2O_4$,[49] CeO_2 (HSA (High surface area), LSA (Low surface area)),[68] Ni-Mg-Al,[69] Ni-Mg/Al and Ni/MgO,[70] $Ni/\gamma\text{-}Al_2O_3$,[71] Pt/Al_2O_3,[72] Au/CeO_2[3] and $TiSmMnO_x$.[73]

2.1.1.3 Sol-gel

The sol-gel is a wet method of catalyst preparation. This technique uses a suspended solid colloidal chemical particle to produce nano-sized particles. A sol-gel is a formation of semi-rigid mass due to the evaporation of the solvent from the sol to form a continuous cross-linked network of particles. Steps in the sol-gel process involve the precursor molecules (organic or inorganic) → Gel formation → Drying process → Calcination → Then the formation of the desired catalyst. This method better controls the catalysts' pore volume, surface area, and pore size distribution. Many nanoparticle catalysts have been prepared using the sol-gel process: Fe/SMC (spherical mesoporous carbon),[74] $Pd/La_2O_3\text{-}CeO_2\text{-}Al_2O_3$,[75] and MnO_x/TiO_2,[76] V_2O_5/TiO_2[77] Co_3O_4,[78] TiO_2/SiO_2[79] and Ag/Co_3O_4.[80]

The hydrothermal synthesis method is a chemical formation technique that produces a catalyst with a single crystal phase that depends on the solubility of precursors in hot water under high pressure. This method has the main advantage of creating a stable crystalline phase at the melting point. This method can control the materials' nucleation and growth to obtain a high homogeneity catalyst to produce

several functional nanomaterials of transition-metal compounds, like oxides, hydroxides, and sulfides.[81] It relies on the hydrolysis of the reactants to produce the oxide ceramics. This is achieved at moderate temperatures (< 200 °C) and high pressures by placing the reagents in a sealed container and heating the system to the reaction temperatures. The solvent is mostly water; a metal hydroxide (*e.g.*, NaOH) is added as a mineralizer, while mineral precursors serve as the source of metal ions. The particle growth results in a catalyst with a good particle-size dispersion.[82] Several catalysts have been prepared via this method: Ag (KCC-1, SBA-15, MCM-41) 67, Mn-Ce/TiO_2 68, Fe-based MOFs,[83] and CoO[84] (KCC: Potassium chloride cotransporter, , MCM: Mobil composition of matter).

2.1.2 Vapor-phase method

2.1.2.1 Pulse spray evaporation chemical vapour deposition (PSE-CVD)

PSE-CVD is a facile, direct, and inexpensive technique for preparing continuous thin film oxides on various substrates without any after-treatment. It can produce films with high purity, uniform thickness, good coverage, negligible damage to the substrate, tuning growth in a selected area, and the increased possibility of using different precursors simultaneously. Co-Mn spinel[85] $CoCuO_x$,[86] Co_3O_4 spinel,[87] α-Fe_2O_3@Fe_3O_4 composite,[88] Cu_2O thin films,[89] Mn_3O_4,[90] and Cu-Fe-Co ternary oxides thin film [91] have been prepared for VOC abatement. Comparing those catalysts, in general, copper exhibits good catalytic performance. Still, Cu-Fe-Co ternary oxides thin film has proved to be an excellent and stable catalyst in catalysis to eliminate VOCs at lower temperatures.

2.1.2.2 Magnetron sputtering

Magnetron sputtering is a fast physical vapor deposition coating method for the deposition of thin films that consist of nanoparticles, metals, and ceramics on a substrate via a high-energy magnetic field on a target material to coat a substrate thin film. Sputtering occurs if the energy transferred in the surface direction is far greater than the surface binding energy (estimated to be equal to sublimation heat). Sputtering of a target atom occurs because of ion bombardment of a surface. Aside from sputtering, another necessary process is the emission of electrons from the target surface. These electrons emitted from the target enable the glow discharge to be continuous.[92] The nanomaterials synthesized via this technique are Chromium-nano-diamond,[93] nanocrystalline Co_3O_4,[94] and Nano-grain $NixCo_{3-x}O_4$ films.[95]

2.1.3 Solid-phase method

2.1.3.1 Flame spray pyrolysis (FSP)

FSP is a fast and economical route to produce nanoparticles in a scalable, one-step manner by combusting organometallic precursors in a self-sustaining flame. Due to its ease of production and versatility, FSP has produced many materials for widespread material applications, such as sensors, paints, and catalysts. This method has been utilized to prepare catalysts with small particle sizes such as: $SiO_2/Ce_{0.7}Zr_{0.5}O_2$,[96] CuO-$TiO_2$,[97] ZnS,[98] Pd/$SiO_2$,[99] Cu/Ce_xZr_{1-x} (x= 0,0.25,0.50, 0.75, 1),[100] CeO_2 [101] and Ce-Mn.[102]

2.1.3.2 Pulsed laser deposition (PLD)

PLD is a solid-phase physical vapor deposition technique that requires a high-energy laser beam to bombard the target reactant inside a vacuum. The material will then be vaporized from the target and deposited on a selected substrate. This technique has been used to prepare nanoparticles and thin-film catalysts for a long time. The following were some of the catalysts synthesized using this technique: Co nanoparticle embedded into Boron thin film catalyst,[103] $CoFe_2O_4$ thin films,[104] $LiMn_2O_4$ thin films,[105] Fe_3O_4 nanoparticles.[106]

During the development of catalyst synthesis, the approach trends have varied from the low-temperature liquid phase to the high-temperature solid phase. Increasing numbers of methods are being reported, and several catalysts have been prepared. Tables 1-3 summarize the primary techniques reported to fabricate catalysts. Their overviews, advantages, and drawbacks have been listed for comparison.

3. Characterization

Different characterization methods have been employed to deeply understand the physico-mechanical properties such as morphology, crystalline phases, chemical composition, surface area, structural stability, and the pore structure of catalysts. Few among those techniques have been discussed in this review paper: X-Ray diffraction (XRD), Extended X-ray Adsorption Fine Structure (EXAFS), X-ray Absorption Near-Edge Structure (XANES), Scanning electron microscopy (SEM-EDS), Transmission electron microscopy (TEM), X-Ray photoelectron spectroscopy (XPS), Brunauer-Emmett-Teller (BET), Hydrogen temperature-programmed reduction (H_2-TPR), Infrared spectroscopy (FTIR), Thermogravimetric analysis (TGA) and DRIFTS (Diffuse reflectance infrared Fourier transform spectroscopy).

3.1 Phase identification

XRD analysis is used to analyze and identify the unknown crystalline compounds. The online standard database (JCPDS database) for the XRD pattern is used as standard for phase identification of various crystalline phases in a catalyst.[107] XRD is also employed to determine crystallinity and assess the phase purity of a material. For example, Tian *et al.* synthesized a pure MnO_4 thin film (see Fig. 3). The prepared catalyst samples have a peaks diffraction at 29.05, 31.04, 32.5, 36.08, 36.5, 44.3, 51.1, 53.91, 58.5, 60.1, and 64.7° which accurately matched with the crystallographic planes of tetragonal Mn_3O_4 (JCPDS No. 24-0734) structure. No peaks relating to other MnO_x phases were detected, indicating the high purity of the final films.[90] XRD is utilized not only to identify the structural changes during the phase transformation

Table 1. Liquid phase method to prepare catalysts.

Preparation method	Overview/Features	Advantages	Drawbacks
Impregnation	Solid support, solvents, metal salts, filtered and dried solid substance, calcination at high temperature.	Technically simple, inexpensive, and few numbers of wastes products.	Controlling Particles size is a challenge, with high tendencies of masking the metal particle
Precipitation	Precursors (nitrate, chloride, acetate), solvents (distilled water, ethanol, cyclohexane), precipitant (NH_4OH, NaOH)	A fast and straightforward method of producing a purely homogeneous catalyst at a low cost	Obtained nanoparticles depending on the pH, temperature, ionic strength properties, toxic liquid waste
Sol-gel	Sol solution, chelating agents, gel formation, calcination	Nanoparticles, large scale, better catalyst control	It is a time-consuming process
Hydrothermal	Single crystals catalyst, low temperature (< 300 ^oC), high pressure. Solvent (distilled water), mineralizer (NaOH).	Pure crystalline phase catalyst, control of the nucleation and growth of the catalyst, homogeneity, environmentally friendly and good dispersion in solution.	Requirement for expensive autoclaves. Safety problem during the reaction process.

Table 2. Vapor phase method to prepare catalysts.

Preparation method	Overview/Features	Advantages	Disadvantages
PSE-CVD	A reliable, fast method for the growth of complex oxides with controlled composition. It offers the potential to produce nano-scale layers of pure metals, metals carbides, and alloys and uses multiple precursors in a single liquid feedstock to grow functionally mixed oxides.	It is a clean, direct, and economical technique for synthesizing thin-film oxides on various substrates without any treatment. It offers potential for producing films with high uniformity of thickness and tailored composition, high purity with a uniform coverage	Low deposition rate, the chance of chemical hazards because of toxic, corrosive, and explosive precursors and gases.
Magnetron sputtering	It uses high energy magnetic field on a target material to coat a thin film of nanoparticles metals, and ceramics on a substrate	High deposition rates, ease of sputtering any metal, alloy/compound, high purity films, very high adhesion of the films to the substrate, excellent surface coverage with uniform film thickness, a potential method to coat heat-sensitive substrates	It is expensive, and the ring magnetic field used forces the secondary electrons to move around the ring magnetic field, plasma instability

but also to check for the purity and improvement of the catalyst.

Ren *et al.* also prepared a range of zinc-substituted hydroxyapatite (Zn-HA) compositions and evaluated the XRD patterns. The results show that the peak's broadness in XRD patterns increased, possibly because of the decreasing crystallinity as a function of the increment in zinc content (5-20 mol% Zn). (As shown in Fig. 4).

XRD also allowed identifying elements and analyzing nanoscale iron precursors isolated with a high degree of crystallinity (Figs. 5a and 5b).

3.2 Structure

EXAFS yields information about the interatomic distances, near-neighbour coordination numbers, and lattice dynamics. On the other hand, XANES gives information about the valence state, energy bandwidth, and bond angles. Yoshida *et al.* employed EXAFS and XANES analysis for the characterization of the rhodium (Rh) species loaded on the NTO (sodium hexatitanate ($Na_2Ti_6O_{13}$)) for the steam reforming of methane.[110] Fig. 6 presents the Rh K-edge XANES, EXAFS, and the Fourier transformed EXAFS spectra of the Rh/NTO (50, 100) and Rh/NTO (100, 100) samples, as well as those of Rh_2O_3 powder and Rh foil as reference samples, before and after the photocatalytic reaction test.

Chen *et al.* employed EXAFS and XANES to reveal the local structure of the Ag atom on the nanostructured hollandite

Table 3. Solid-phase method of catalysts preparation.

Preparation method	Overview/Features	Advantages	Disadvantages
Flame spray pyrolysis	It involves combusting an organometallic precursor in a self-sustaining flame to produce a nano-catalyst.	The fast and economical route, nanoparticles, large scale, one-step process, suitable particle size, and high specific surface area.	Not easy to scale up (yield is meagre), catalysts with high porosity (10-20 vol%), low density, and high oxides levels for metal deposits (10-20 wt%).
Pulsed laser deposition	The high-energy laser beam to bombard a target reactant, thin-film catalyst, the rate of the thin film growth can be controlled by changing background gas, adjusting the laser parameters, deposition time, and substrate to target distance.	Flexibility in manufacturing high-grade coatings material for thermal and corrosion barriers, easier to obtain film stoichiometry for multi-element materials very short time frame deposition,	Relatively expensive; the large kinetic energy, non- uniformity of the particle size across the surface of the film.

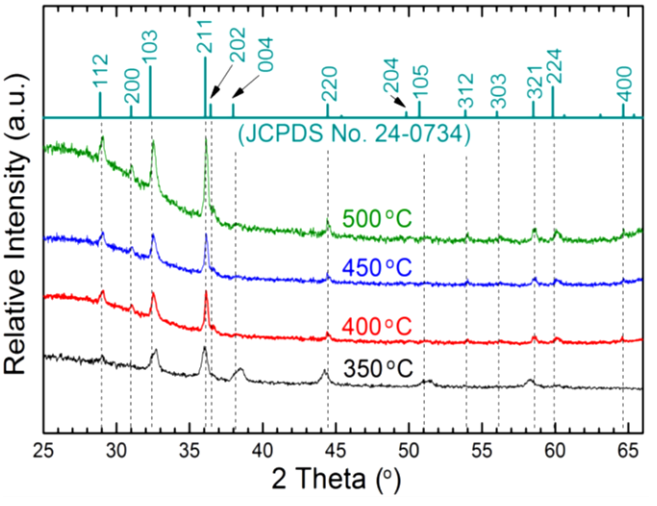

Fig. 3 XRD patterns of Mn_3O_4 films (thickness of ~300 nm, corresponding to JCPDS card No. 34-0734) deposited on silicon at different substrate temperatures. Reproduced with the permission from[90], Copyright 2013 American Chemical Society.

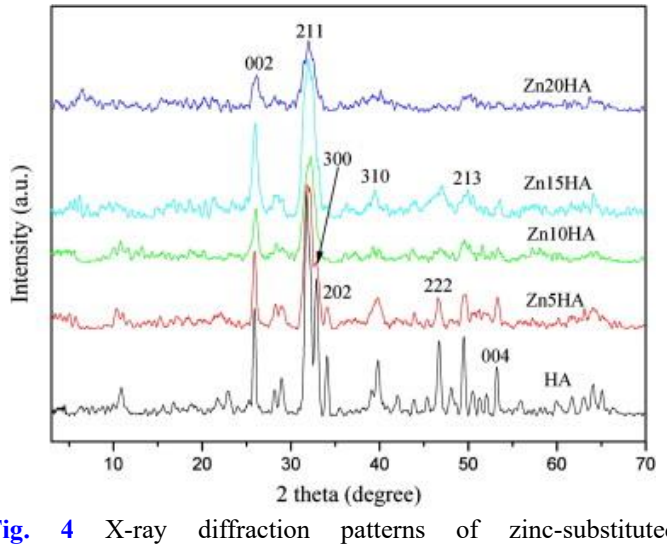

Fig. 4 X-ray diffraction patterns of zinc-substituted hydroxyapatite (Zn-HA). Reproduced with the permission from[108], Copyright 2009 Acta Materialia Inc.

manganese oxide (HMO) surface for benzene oxidation.[111] Figs. 7a and 7b illustrate the EXAFS data at the Ag K-edge and XANES spectra. The FT amplitude of the EXAFS spectrum of Ag_1/HMO in 2.8-3.0 Å outstanding to the scattering between the Ag atoms is absent (Fig. 7a). This reveals the isolated states of the Ag atoms. The first two shells, with distances of ~2.35 and ~2.62 Å and coordination numbers of 4 and 1, involve that the isolated Ag atoms are anchored on HMO surfaces. XANES spectra in Fig. 7b show that their metallic states are retained when isolated Ag atoms are created on HMO surfaces. The absorption threshold energy (E_0) of Ag_1/HMO is ~25514 eV, which is close to the E_0 value of Ag foil and higher than E_0 of Ag_2O, confirming the presence of $Ag^{\delta+}$ in Ag_1/HMO ($0 < \delta < 1$).

3.2 Morphology and bulk composition

SEM, TEM, and EDS are the techniques utilized to determine the morphology and bulk composition of the as-prepared catalysts for catalytic application. SEM uses a beam of focused electrons to examine the surface morphology and structural features of a nanomaterial. The focused electrons interact with the different atoms present at the surface of the catalyst material, producing various signals to image the information at the catalyst surface. For example, Fig. 8 presents the SEM images of the-Fe_2O_3 thin film synthesized by Kouotou *et al.* at different temperature ranges. They employed the SEM analysis technique to observe the changes in the structure. From 300 °C to 400 °C, the images display small grains morphology embedded in the structure and are evenly closely packed octahedral shape with grains (~60 nm) composed of pallet shaped crystals overlaid on each other in detailed orientation. While at 450 °C, the film exhibits needle-like structures, each of which could result from the incorporation and aggregation of small individual particles. The Authors reported that the significant changes of film morphology have been beneficial for the deep propene oxidation reaction.

SEM coupled with EDS allowed the surface morphology

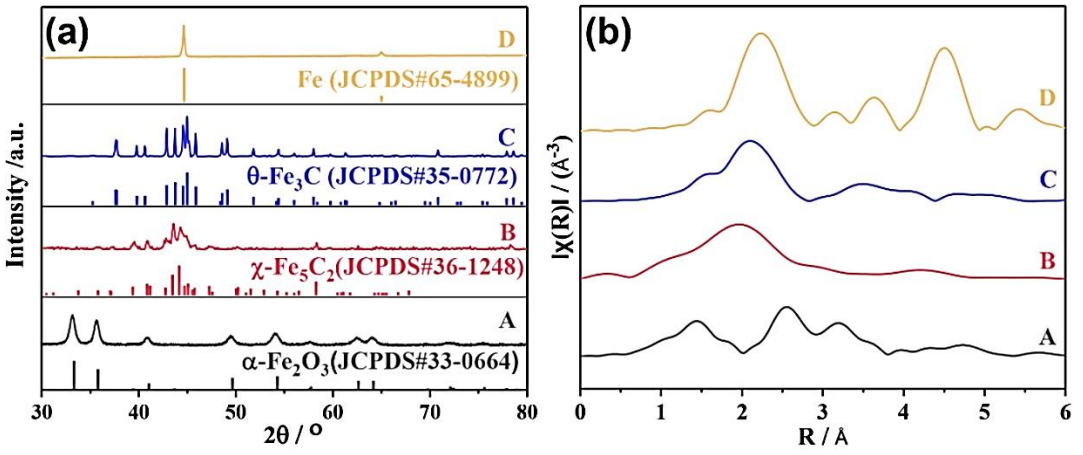

Fig. 5 Characterization of catalysts precursors and used catalysts: (a, b) experimentally obtained XRD patterns and k2-weighted Fourier transformed Fe K-edge EXAFS data of precursors; (c, d) XRD patterns of used catalysts under condition 1 and condition 2. Reproduced with the permission from[109], Copyright 2013 American Chemical Society.

analysis and quantified the elemental composition (Fig. 9). Fig. 9a shows that the Cu/CeO_2 material consists of agglomerates of lighter, larger particles (marked as Z1) and darker, more minor parts (marked as Z2). The more delicate parts correspond to Ce-rich areas Fig. 9b, whereas the darker ones to Cu-rich phases Fig. 9c. A closer detail is depicted in Fig. 9d, showing that the material has a "cloud-like" appearance. Closer details of Cu/Gd_2O_3 is demonstrated in Fig. 9e, showing some features that resemble "desert-rose" petals. The same is observed in Fig. 9f, where distinct darker (Z1) and lighter (Z2) zones correspond to Cu-rich Fig. 9g and Gd-rich Fig. 9h phases, respectively.[58]

Atomic resolution TEM is mainly used to study the detailed structural atomic-scale information of single-atom catalysts and the interactions between metals and supports. This technique is essential for understanding the reduced catalyst's catalytic performance and degradation mechanisms. As shown in Fig. 10, the SiO_2@Ni@ZrO_2 catalyst exhibits a core-shell structure. The surface of silica spheres is decorated with Ni nanoparticles, which have a size of 6 nm. The Ni nanoparticles decorated silica spheres are covered with porous ZrO_2 shells. As shown in Figs. 10c–g, most Ni nanoparticles are incorporated between the silica core and zirconia shell. It is noted that a few Ni nanoparticles separated from the silica surface (Fig. 10d). By examining the region of separated Ni nanoparticles, both silica and zirconia are also present and encapsulate the Ni nanoparticles (Figs. 10c and 10e).[67]

The microstructure of the catalysts can also be characterized by TEM. As shown in Fig. 11a, Fe-based nano-polyhedrons with a diameter in the range of 30−40 nm were shown to be uniformly dispersed on the carbon carriers; also, the MOF derived Fe-based nano-polyhedrons show encapsulation by a few carbon layers (Fig. 11b), which is effective to inhibit the undesirable aggregation during the CO_2 conversion. The scanning TEM (STEM) and EDS mapping images of the used Na-Fe@C confirmed the homogeneous distribution of Fe-based nano-polyhedrons and Na on the substrate (Fig. 11c).[83]

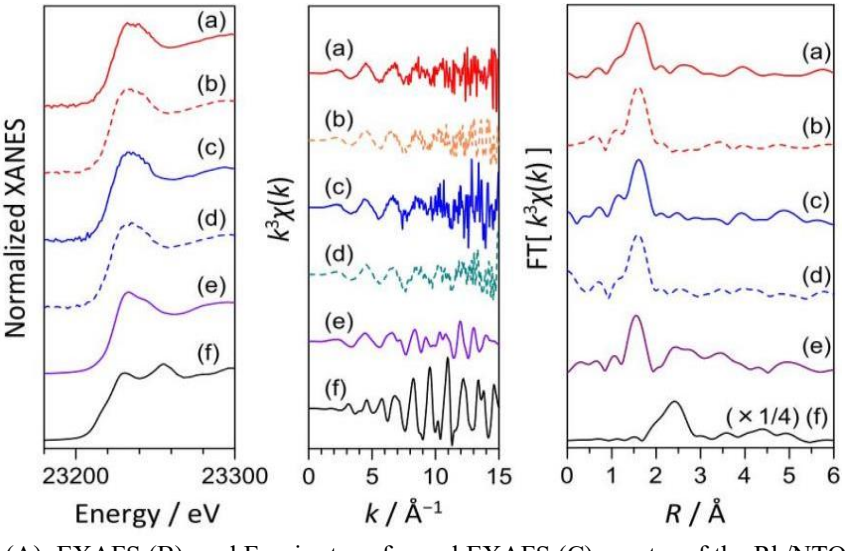

Fig. 6 Rh K-edge XANES (A), EXAFS (B), and Fourier transformed EXAFS (C) spectra of the Rh/NTO (50,−100) samples (a, b) and the Rh/NTO (100,−100) samples (c, d) before (a, c: solid lines) and after (b, d: broken lines) the photocatalytic reaction test, and those of Rh_2O_3 (e) and Rh foil (f) as the reference samples. Reproduced with the permission from[110] Copyright 2019 Elsevier B. V.

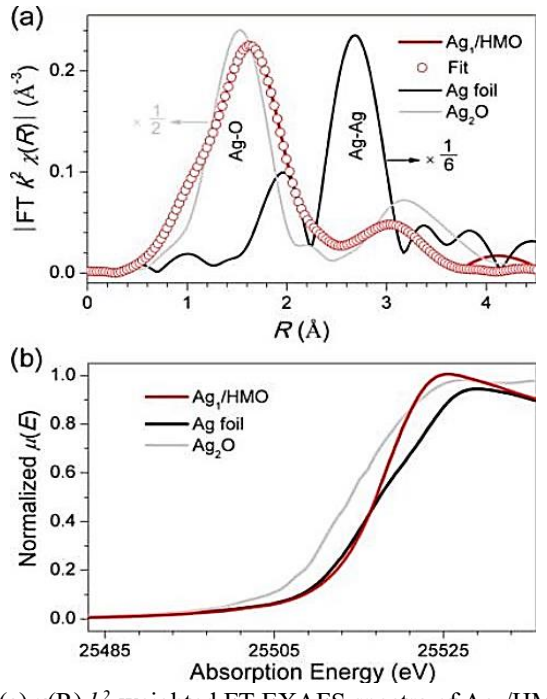

Fig. 7 (a) χ(R) k^2-weighted FT EXAFS spectra of Ag_1/HMO, Ag foil, and Ag_2O. (b) Ag *K*-edge XANES spectra of Ag_1/HMO, Ag foil, and Ag_2O. Reproduced with the permission from[112], Copyright 2017 American Chemical Society.

Fig. 12a shows the representative TEM image of the Pt1@CeO_2 catalyst with ~0.5 wt% of Pt. The exhibition has a slab-like morphology with the size varying from ~15 to ~40 nm, likely transformed from the porous nanospheres. The high-resolution HAADF-STEM images reveal that Pt is dispersed on the CeO_2 nano-slabs at the atomic scale (Figs. 12b-d). Individual Pt atoms are exhibited as bright dots with higher contrast in these images than the surrounding CeO_2 lattice (Figs. 12e and f). The slab-like nanocrystals exhibit

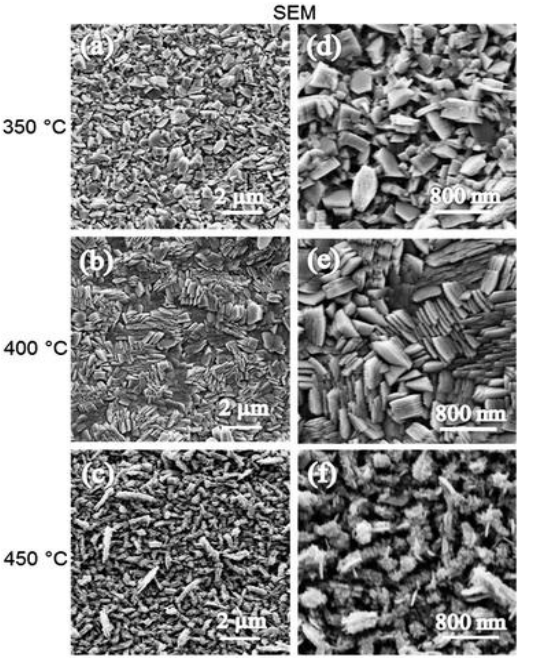

Fig. 8 SEM images of a-Fe_2O_3 thin films coated on stainless steel at: (a and d) 350 °C, (b and e) 400 °C, and (c and f) 450 °C. Reproduced with the permission from[111], Copyright 2013 Royal Society Chemistry.

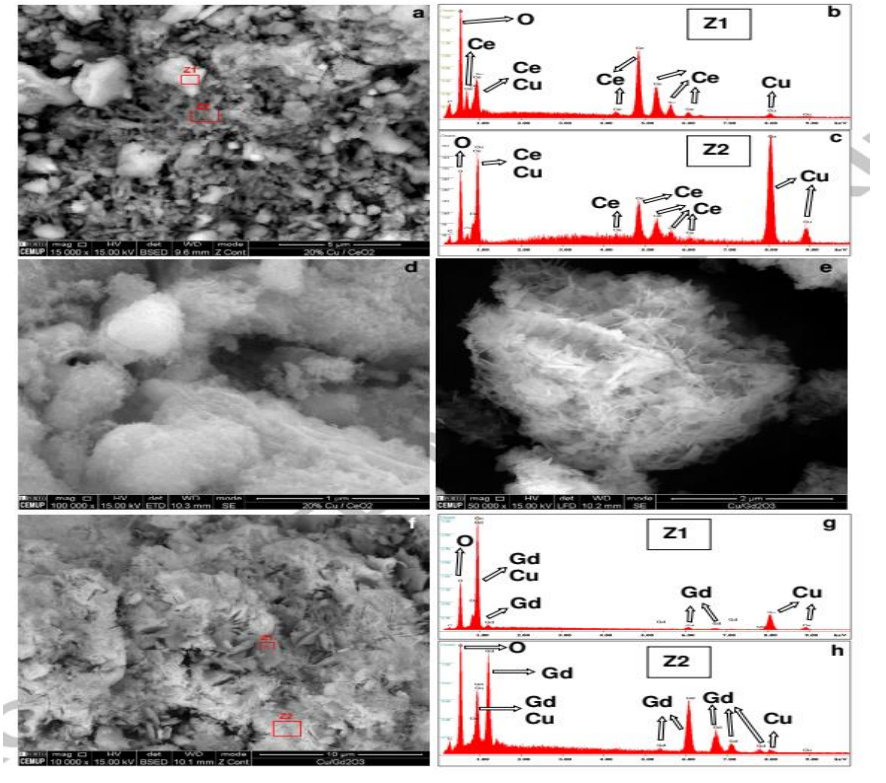

Fig. 9 SEM images Cu/REO samples: Cu/CeO_2 (a) with respective EDS spectra of zones marked as Z1 (b) and Z2 (c) and a closer detail (d); Cu/Gd_2O_3 in closer detail (e) and a general view (f) with respective EDS spectra of zones Z1 (g) and Z2 (h). Reproduced with the permission from[58], Copyright 2016 Elsevier B.V.

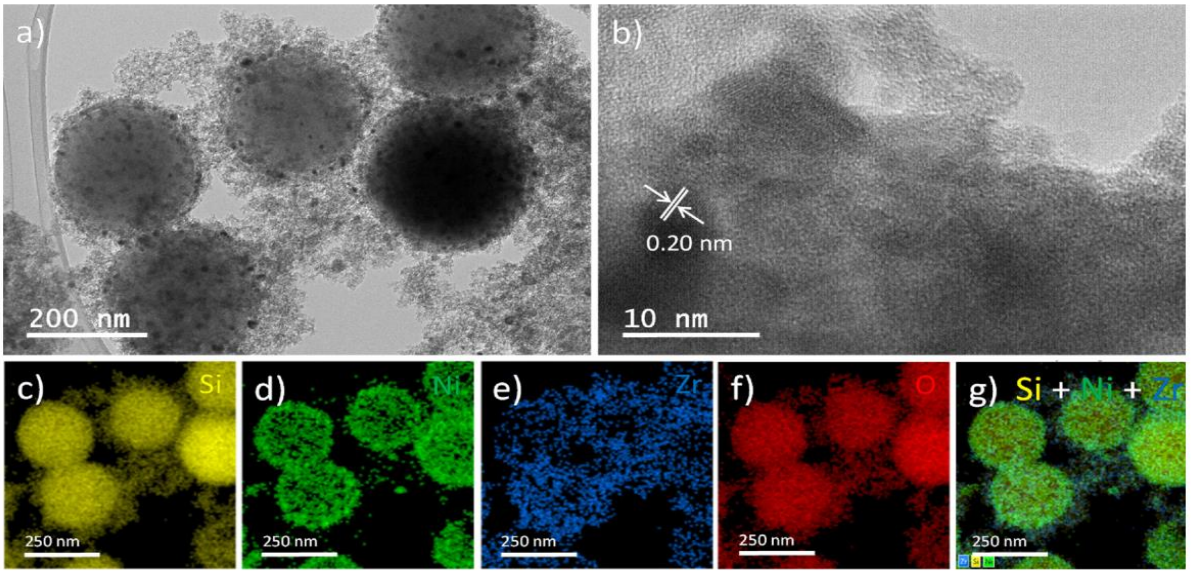

Fig. 10 (a, b) TEM images and (c–g) EDX mapping of reduced SiO2@Ni@ZrO2 catalysts. Reproduced with the permission from[67], Copyright 2016 Elsevier B.V.

lattice fringes with a spacing of ca. 0.31nm, which can be assigned to the (111) planes of CeO_2 in the fluorite phase (Fig. 12b).[20]

3.3 Specific surface area

An N_2 desorption experiment carries out BET analysis to study the surface area of prepared catalysts and their effect on the catalytic application; for instance, Lasiripojana *et al.* used the BET analysis method to study the effect of calcination temperature on the surface area of the CeO_2 catalyst for dry catalytic reforming of methane.[68] Their findings show that the surface area decreases with calcination temperature.

Zhang *et al.* also employ BET analysis techniques to observe the cumulative effect of manganese oxides on titanium oxides on the surface area, pore volume, and pore size for coal combustion application using supported manganese oxides on titanium oxides.[76] It is observed that the introduction of manganese oxides greatly enlarged the surface areas due to MnO_x being doped into the TiO_2 structure. This occurrence provided additional nucleation sites and controlled the sintering and pore plugging of TiO_2.

3.4 Redox properties

H_2-TPR is usually used to observe the redox property of the catalysts. H_2-TPR is a characterization technique to study the nature of catalyst reduction with temperature change. The H_2-TPR profiles shown in Fig. 13 reflect the reduction behavior of oxidized species of CoO catalysts with no prominent reductive peaks below 600 °C for OMSC4 compared with the CoO catalysts indicating the negligible catalytic effect on the support in Fischer Tropsch synthesis. The catalysts simultaneously present three reductive peaks. The two peaks at about 300 °C and 500 °C are assigned to the reduction from Co_3O_4 to CoO and CoO to Co, respectively.[43]

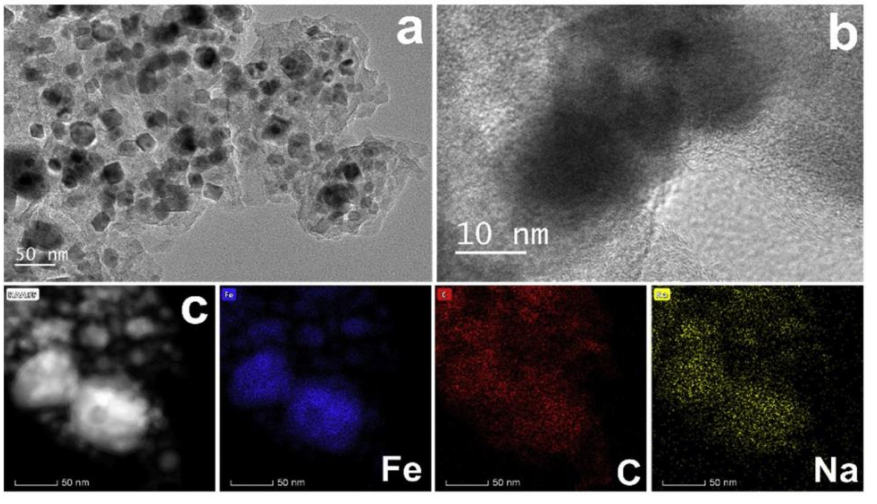

Fig. 11 (a) TEM and (b) High-Resolution TEM (HRTEM) images of the used Na-Fe@C catalyst. (c) STEM image of the used Na-Fe@C and the corresponding elemental mapping of iron (Fe), carbon (C), and sodium (Na) elements. Reproduced with the permission from[83], Copyright 2016 Elsevier B.V.

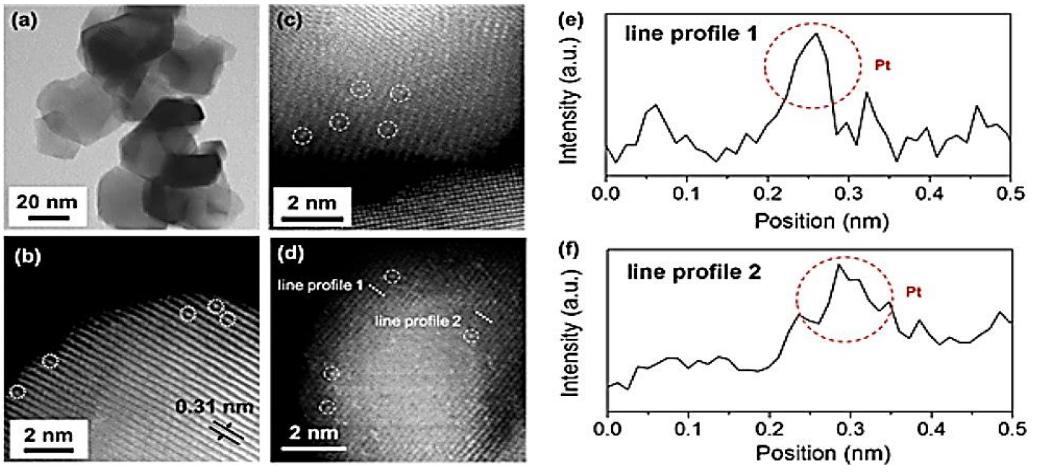

Fig. 12 Representative (a) TEM and (b-d) high-resolution HAADF-STEM images of the Pt1@CeO_2 catalyst with 0.5 wt% of Pt. (e, f) Intensity profiles of the scans along the dash lines marked in (d). Reproduced with the permission from[20], Copyright 2016 Elsevier B.V.

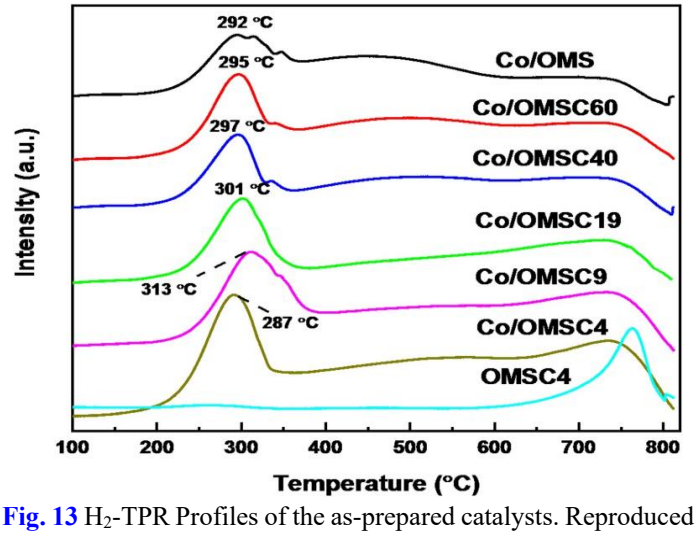

Fig. 13 H_2-TPR Profiles of the as-prepared catalysts. Reproduced with the permission from[111], Copyright 2020 Dalian Institute of Chemical Physics, the Chinese Academy of Sciences.

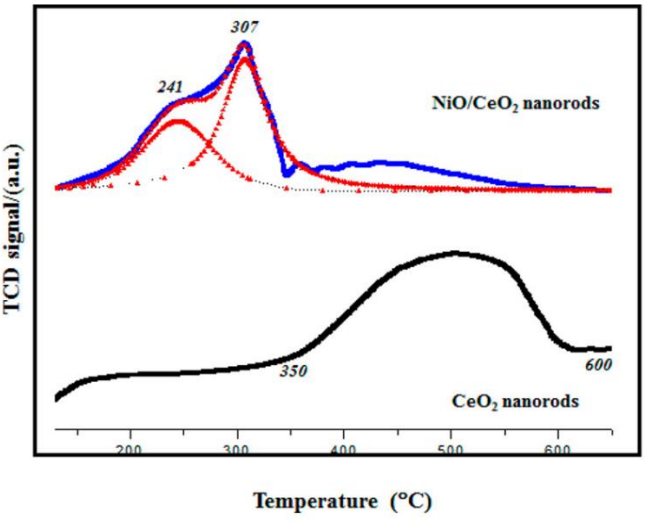

Fig. 14 Reducibility temperature of the NiO/CeO_2 (blue line) and CeO_2 (black line) nanorods by H_2-TPR measurement. Reproduced with the permission from [112], Copyright 2020 Dalian Institute of Chemical Physics, the Chinese Academy of Sciences.

In 2014, Maitarad et al. employed the H_2-TPR to study the effect of NiO on the reduction properties of CeO_2 nanorods for the selective catalytic reduction of NO with NH_3.[112] The H_2-TPR results of CeO_2 and NiO/CeO_2 nanorods are shown in Fig. 14. In the temperature range of 350–600 °C, CeO_2 nanorods show broad reduction peak profiles, which corresponds to the reduction of Ce^{4+} to Ce^{3+}. Two distinct hydrogen-consumption peaks were identified when a small quantity of NiO was added to the CeO_2 nanorods. The reduction of NiO nanoparticles and surface ceria nanorods are responsible for the significant peak at 307 °C. Another peak at 241°C is due to a decrease in adsorbed oxygen on the surface, which could be due to the short radius of Ni that can incorporate into the surface of the ceria nanorods. As a result, the H_2-TPR peak profile clearly demonstrates that adding Ni to CeO_2 nanorods lowers the temperature of their catalytic reducibility compared to pure CeO_2 nanorods. This suggests that the interaction between nickel and cerium oxides is favored, resulting in improved NO conversion at lower temperatures.

3.5 Elemental compositions and oxidation states

XPS is also denoted as electron spectroscopy for chemical analysis (ESCA). It is a surface analysis technique that can measure the electronic state, elemental composition, chemical state, and empirical formula of the elements within the surface of a material. The XPS spectra work based on the bombardment of the solid surface with a beam of X-rays while at the same time measuring the kinetic energy of the emitted electrons from the top 1-10 nm of the material.

To deeply understand the catalytic performance of Ni-Si/ZrO_2 and Ni-Zr/SiO, Wang *et al*. careful carried out an XPS analysis to gain an insight into which element plays a significant role during the reaction, especially investigated the state of Ni, Si, and Zr[57] and the results are shown in Fig. 15. XPS measurements were carried out for the Cu/Ce1−xSmxO1 samples to gain the surface and elemental state information.

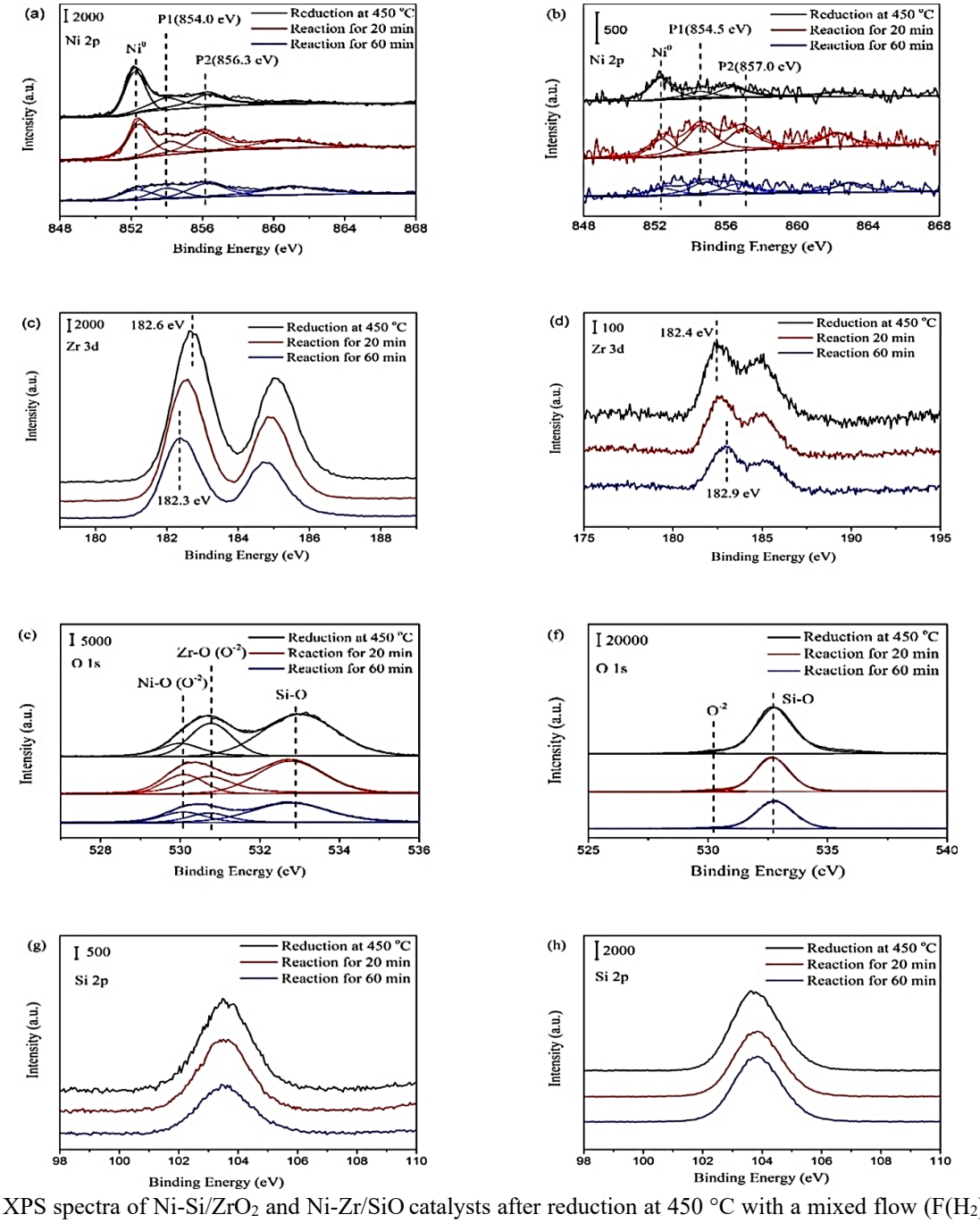

Fig. 15 In situ XPS spectra of Ni-Si/ZrO_2 and Ni-Zr/SiO catalysts after reduction at 450 °C with a mixed flow (F(H_2) = F(Ar) = 30 mL min-1) and reaction at 400 °C with a mixed flow (F(CH_4) = F(CO_2) = 30 mL min-1): (a) Ni2p, (c) Zr3d, (e) O1s, and (g) Si2p for Ni-Si/ZrO_2 catalyst and (b) Ni2p, (d) Zr3d, (f) O1s, and (h) Si2p for Ni-Zr/SiO_2 catalyst. Reproduced with the permission from[57], Copyright 2018 American Chemical Society.

Fig. 16 depicts the XPS spectra in the Cu2p region for the catalysts with different Ce/Sm atomic ratios. All spectra are characterized by two main peaks of Cu2p1/2 (952.5–954 eV) and Cu2p3/2 (932.2–934.2 eV), along with shakeup satellite peaks centered at 942.2–944.9 eV. The Cu/CeO_2 sample (x = 0) is characterized by a Cu2p3/2 band at 934.1 eV, which can be ascribed to oxidized Cu^{2+} species. The latter is further confirmed by shake-up satellites at 944.5 eV, typical of Cu^{2+} species. At a Ce/Sm ratio of 3 (x = 0.25), the intensity of the Cu2p3/2 peak decreases, and no shift is found, implying a decrease of Cu^{2+} species on the surface of the Cu/$Ce_{0.75}Sm_{0.25}O_{1.875}$ sample. When the Ce/Sm atomic ratio is 1 (x = 0.5), both the band at high BE values (934.1 eV) and the shake-up peaks are attenuated, suggesting a smaller contribution of Cu^{2+} species to the overall intensity.[113]

3.6 Thermal stability

TGA is generally conducted on a powder catalyst sample to detect the changes in weight with temperature changes and measure thermal stability, moisture composition, oxidative stability, volatile content, kinetic decomposition, sample dehydration, and life span. Fig. 17 depicts TG curves for the

decomposition of MnO_2 to Mn_2O_3. The M2 sample is still losing water moisture even at 800 °C due to the OH-groups in the oxide bulk.[114]

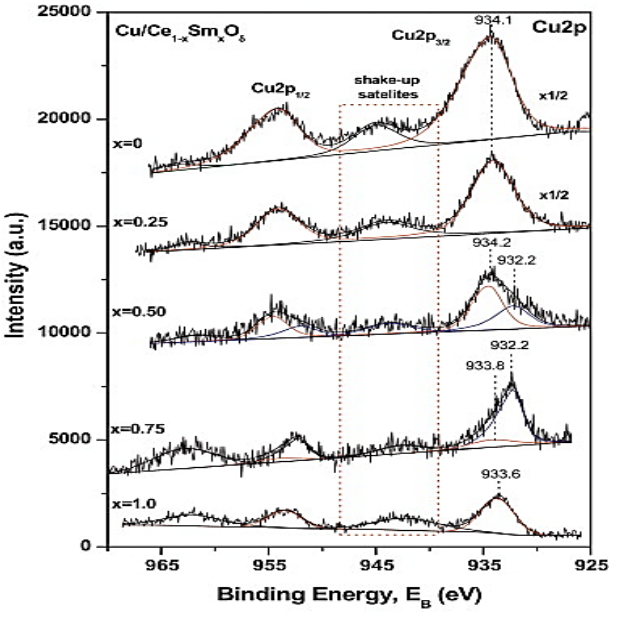

Fig. 16 XPS Cu2p spectra of $Cu/Ce_{1-x}Sm_xO_\delta$ catalysts. Reproduced with the permission from[57], Copyright 2018 American Chemical Society.

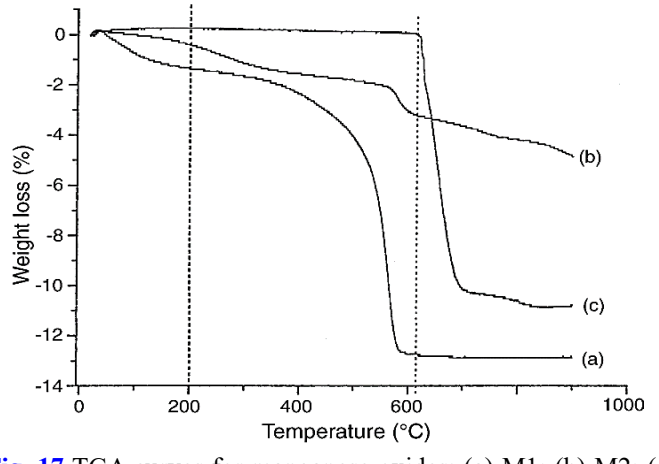

Fig. 17 TGA curves for manganese oxides: (a) M1; (b) M2; (c) M3. Reproduced with the permission from[114], 2005 Elsevier B.V.

Boudjeloud *et al.* have employed the TGA analysis technique to study the dehydration and degradation of respectively non-calcined Ni/Al and Ni-La/Al gels before calcination catalyst for steam reforming of methane,[115] as shown in Fig. 18. A total loss of 18.5wt% of the thermal degradation of Ni nitrates with the ratio Ni/Al was reported around three intervals temperature. The first decomposition step at a 25 to 189 °C temperature range is assigned to the degradation of Nickel nitrates leading to lower hydrates formation. The second loss, located from 189 to 382 °C, characterizes the nitrates degradation. At the last step over 382 °C, the TGA profiles become steady, conducting to the formation of Ni oxide.

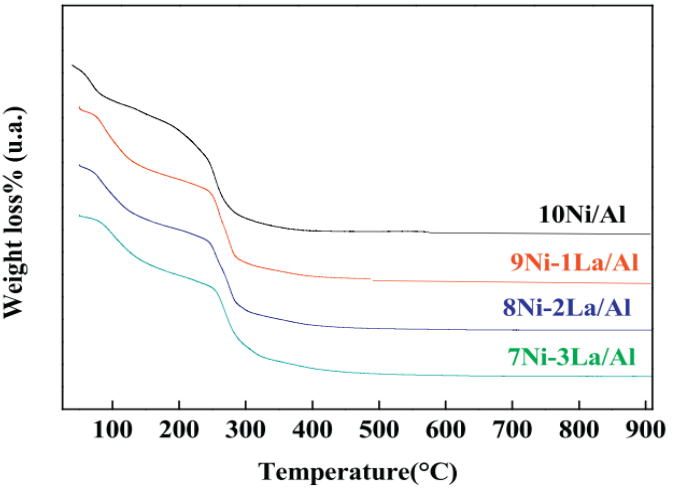

Fig. 18 TGA curves of Ni/Al and Ni-La/Al samples. Reproduced with the permission from[115], Copyright 2019 Hydrogen Energy Publications LLC.

3.7 Mechanism information

DRIFTS is an infrared spectroscopy sampling technique for powders materials. The infrared light is reflected and transmitted in varying amounts on a sample depending on the bulk properties. To get a more comprehensive evaluation of the atomic dispersion of Pt, Xie *et al.* used DRIFTS to examine $Pt_1@CeO_2$ Catalysts for direct methane conversion. Xie *et al.* have proved the DRIFTS approach to identify single Pt atoms on oxide supports.[116] Fig. 19 shows the adsorption spectra obtained on $Pt_1@CeO_2$ catalysts with varying Pt loadings (0.25, 0.5, and 1.0 wt%) and $PtNPs/CeO_2$ (0.5 wt%), where CO was pre-adsorbed at different partial pressures. For the $Pt_1@CeO_2$ catalysts with 0.25 and 0.5% of Pt (Figs. 19a and b), only one peak was detected at 2089 cm^{-1}, attributed to Pt^+'s linearly bound CO (CO_L) on Pt^+. Additional peaks at 1991 cm^{-1} can be found in 1.0% $Pt_1@CeO_2$ (Fig. 19c) and $PtNPs/CeO_2$ (Fig. 19d), which can be attributed to bridge bonded CO (CO_B) on Pt, which is a common property of Pt ensembles with continuous surfaces. The lack of the CO_B peak demonstrates that Pt sites are isolated in $Pt_1@CeO_2$ catalysts at low Pt ratios (*e.g.*, < 1%), whereas Pt clusters develop at larger loadings.

Many researchers have used in situ DRIFTS in the past years to provide a possible reaction mechanism. Fan *et al.* have employed in situ DRIFTS to reveal the possible catalytic mechanism over the prepared CoO_x VOCs oxidation.[117] As shown in Fig. 20, spectra recorded below 200 °C revealed a prominent C_3H_6 (913 cm^{-1}) adsorption peak. As the temperature rises, the C_3H_6 adsorption peak tends to disappear, while the CO_2 peak at 669 cm^{-1} gets stronger. This means that C_3H_6 is initially adsorbed on the CoO_x catalyst's surface, and the reaction rate of adsorbed C_3H_6 accelerates with temperature's increment, and more CO_2 is produced throughout the catalytic process. The adsorption peak of C_3H_6 grows weaker, and the CO_2 peak becomes stronger as the rate of C_3H_6 consumption and thus CO_2 production increases. Adsorption of C_3H_6 on CoO_x thin film was observed using in

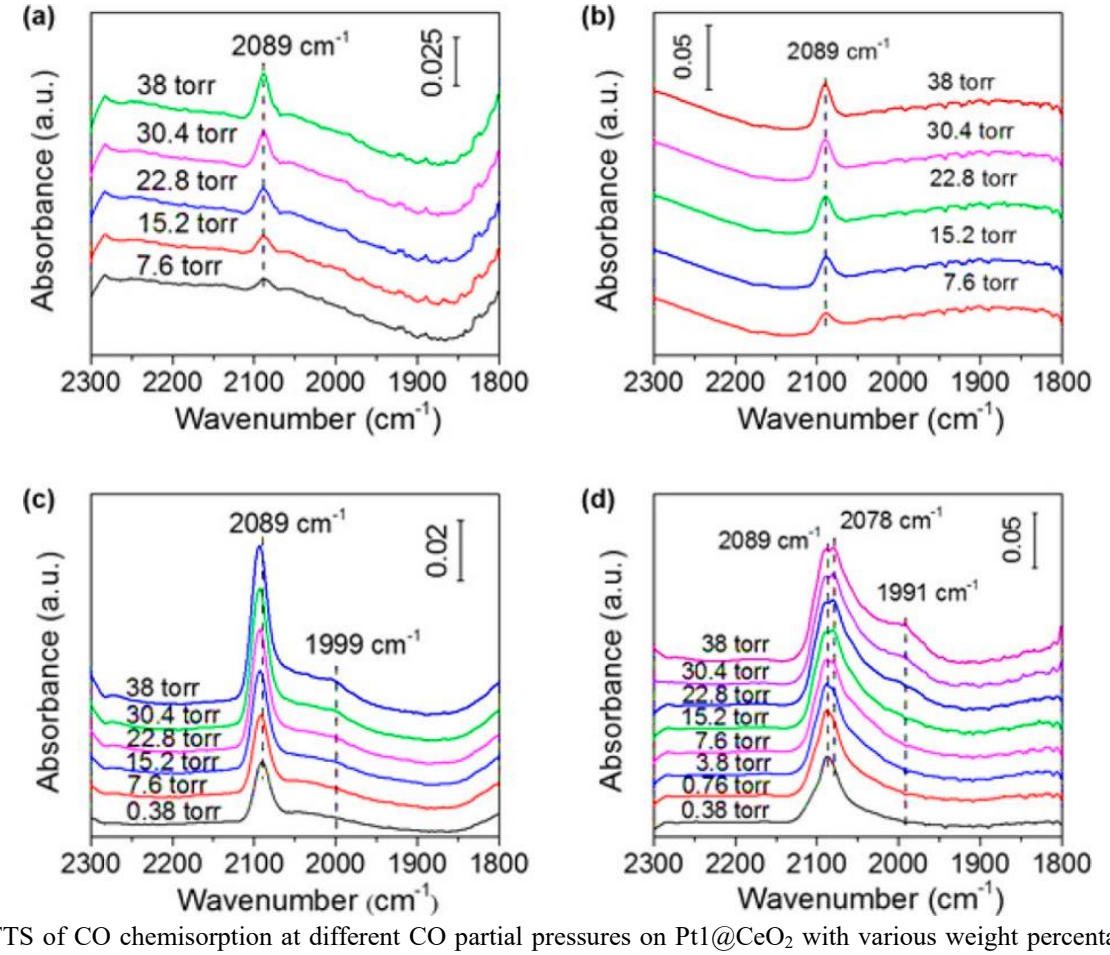

Fig. 19 DRIFTS of CO chemisorption at different CO partial pressures on Pt1@CeO_2 with various weight percentages of Pt: (a) 0.25%, (b) 0.5%, and (c) 1.0%. (d) PtNPs/CeO_2 (0.5 wt %) was also shown for comparison. Reproduced with the permission from[116], 2018 American Chemical Society.

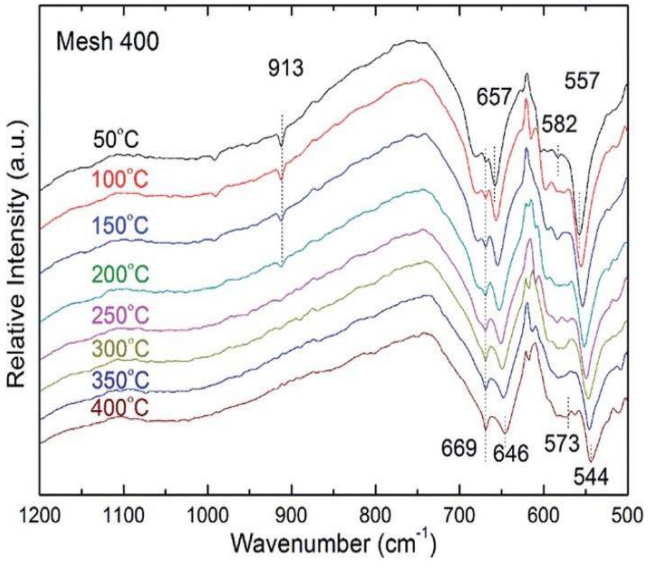

Fig. 20 In situ DRIFTS spectra of CoO_X prepared at 400 °C during C_3H_6 oxidation at different temperatures. Reproduced with the permission from[117], Copyright 2015 RSC Publishing.

situ DRIFTS spectra, implying that the Langmuir-Hinshelwood (L-H) mechanism precedes the catalytic reaction of C_3H_6 on CoO_x.

De Oliveira Rocha *et al*. have performed DRIFTS with CO (DRIFTS-CO) to investigate the effect of Au doping on Ni/Al_2O_3 catalysts during methane steam reforming.[118] An understanding of the modifications of a real Ni catalyst's surface structure following the addition of Au was revealed. DRIFTS-CO spectra for the *x*AuNiAl samples following CO exposure are presented in Fig. 21(A) 2200-1700 cm^{-1}. After purging with N_2 at 300 K, Fig. 21(B) displays the spectra.

4. Reaction kinetics and mechanism

4.1 DFT calculations

DFT (Density functional theory) calculation is generally performed to predict the reaction pathway, the partial density of state, transition state, rate constant, detect the properties of a material, and confirm the experimental data to gain more insight into the material.

For example, the performances of Single-site Catalysts (SSCs), and Ni/MgO (Fig. 22) for the methane reforming reaction was systemically studied by combining theoretical modeling and experimental studies. The DFT calculations in (Fig. 23) show that synergy between a single Ni atom and MgO in the SAC Ni_1/MgO is not active due to the reaction intermediates' weak bindings as that of MgO and the limited amount of adjacent active sites. It was confirmed by the

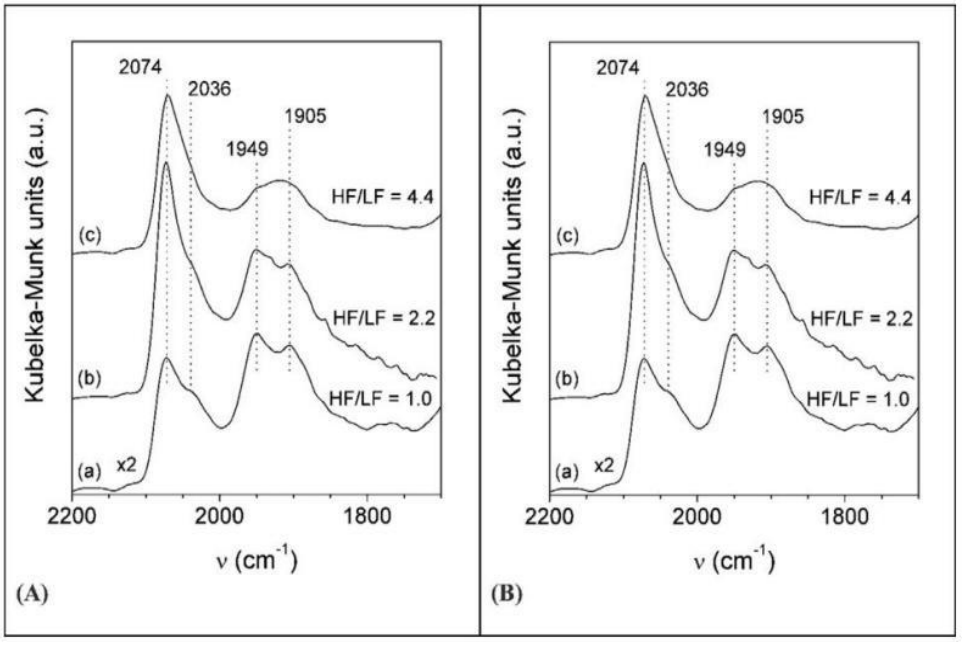

Fig. 21 DRIFTS-CO spectra of samples (a) NiAl, (b) 0.55AuNiAl, and (c) 1.2AuNiAl, at room temperature, after desorption (A) and after purging with N_2 for 10 min (B). Reproduced with the permission from[118], Copyright 2019 Elsevier Ltd.

experimental data on the 2.5% Ni/MgO catalyst and a tiny Ni cluster atom. According to the KMC (Kinetic Monte Carlo) simulations (Fig. 23), the site confinement of SSCs Ni4/MgO helps balance the activations of CO_2 and CH_4, which is essential to achieving the yield and the H_2/CO ratio and preventing poisoning of active sites during the dry reforming reaction.[66]

Recently Qiu *et al*. utilized DFT calculations to solve the carbon deposition problem on the Ni catalyst for dry reforming of methane (DRM) via deposition of several proportions of Cu on Ni (111) surface, Cu_1Ni_8, and Cu_6Ni_3. They described that Cu doping into Ni (111) surface weakens the surface-adsorbate interaction and decreases the CH dissociation energy barrier. The Cu_6Ni_3 surface displayed the greatest carbon resistance since the C-H bond is more easily consumed via oxidation than direct dissociation[119] depicting that pure Ni (111) has the lowest energy of 1.3 eV, with the heat of reaction of 1.14 eV, signifying that CH is more likely to crack on the pure Ni (111) surface compared with Cu_1Ni_8 and Cu_6Ni_3 kinetically. The occurrence enlightens why adverse carbon deposition frequently occurs on Ni catalysts. The replacement of one Cu atom and six Cu atoms into the Ni (111) surface can increase the activation energy by 0.07 eV and 0.2 eV, respectively, indicating that the addition of Cu is kinetically unfavorable to this reaction, seen in Fig. 24.

Maitarad *et al*. performed DFT calculations to evaluate the complete catalytic cycles of NO conversion on the Si single atom doped in four pyridine N at the divacancy site of graphene.[120] They found that SiN_4G is more reactive to NO adsorption than CO and is unresponsive to the water effect. Adsorption energy (E_{ad}) of different species was calculated using the equation below:

$$E_{ad} = E^{complex}_{adsorbate-substrate} - E^{isolate}_{substrate} - E^{isolate}_{adsorbate} \quad (1)$$

where $E^{complex}_{adsorbate-substrate}$, $E^{isolate}_{substrate}$ and $E^{isolate}_{adsorbate}$ are total energies of an adsorbate-substrate complex, a bare surface, and an isolated adsorbate, respectively.

The adsorption strength of gas over SiN_4G followed the calculated E_{ad} values as: NO_2 (-3.20 eV) > O_2 (-2.96 eV) ≫ NO (-1.94 eV) ≫ N_2O (-0.97 eV) > CO (-0.66 eV) > H_2O

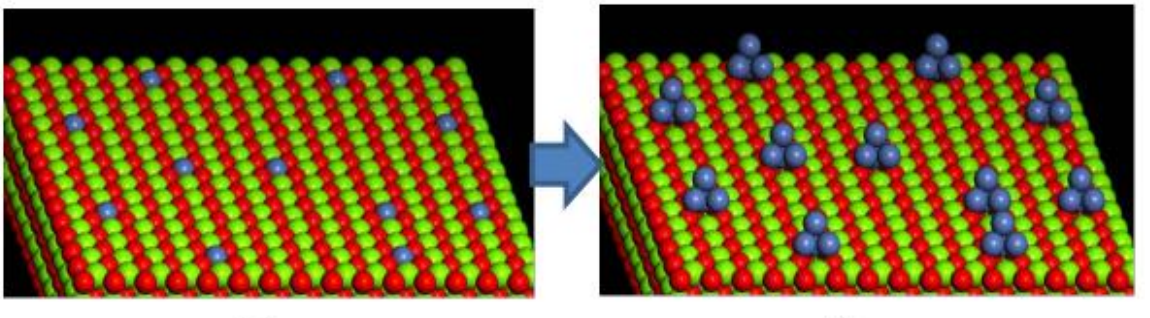

Fig. 22 Schematics of structures for single-atom Ni_1/MgO (100) catalyst (a) and single-site Ni_4/MgO (100) catalyst (b). Green: Mg; Red: O; Blue: Ni. Reproduced with the permission from[66], 2018 American Chemical Society.

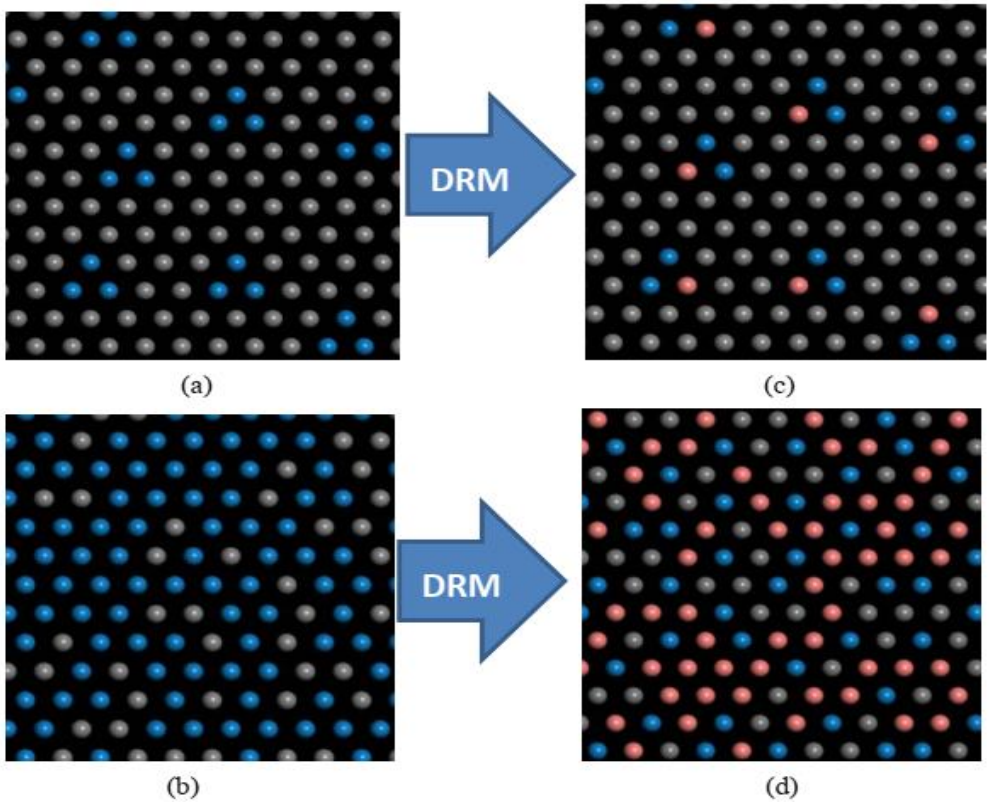

Fig. 23 KMC-simulated surface matrix for the Ni_4/MgO (100) with (a, c) and without site confinement (b, d) before (a, b) and during the DRM reaction at 700 °C and 1 atm with CO_2:CH_4 ratio of 1 (grey: MgO, blue: Ni, red: *O). Reproduced with the permission from[66], Copyright 2018 American Chemical Society.

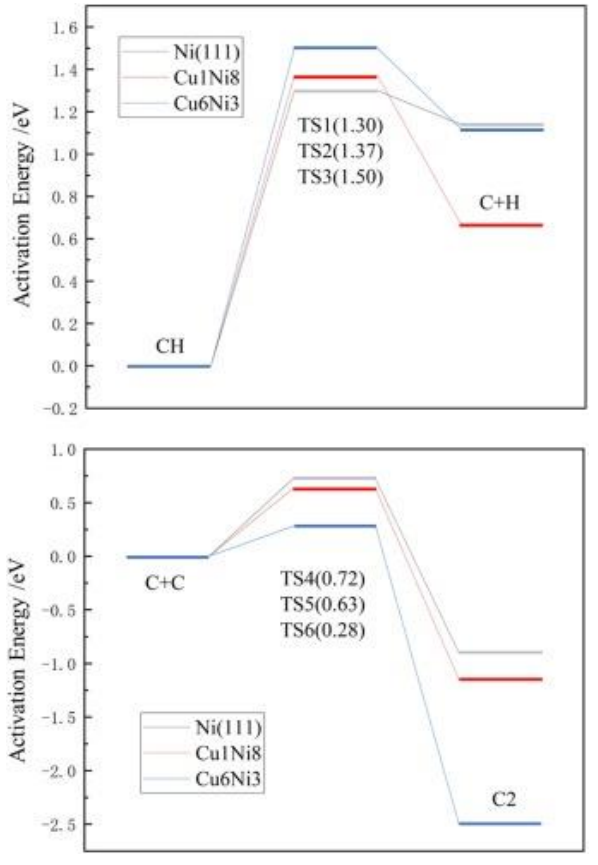

Fig. 24 The energy profile of carbon formation. Reproduced with the permission from[119], 2019 American Chemical Society.

(-0.56 eV) > CO_2 (-0.37 eV) > N_2 (-0.17 eV). A negative E_{ad} value indicates the attractive interaction between the surface and the adsorbate in the complex in terms of stability. The calculated E_{ad} values of selected configurations and adsorption structures are given in Fig. 25.

Pei *et al.* have carried out density functional theory calculations to present the difference in the IB-metal-alloyed Pd single atoms.[121] Their results (see Fig. 26) showed that electron transfer from Cu or Ag to Pd occurred when the Cu or Ag-alloyed Pd single-atom catalyst was formed. They negatively affected Pd atoms (-0.37e and -0.22e, respectively). Moreover, the electron might be transferred from Pd to Au in the Au-alloyed Pd single-atom catalyst. This was also following the order of their electronegativity: Au (2.54) > Pd (2.20) > Ag (1.93) ≈ Cu (1.90).

4.2 Mechanism in catalysis

4.2.1 Mechanisms of catalytic oxidation of VOCs

To describe the reaction pathway in VOCs abatement, the following reaction mechanisms were proposed:

- Mars-van Krevelen (MVK) mechanism;
- Langmuir–Hinshelwood (L-H) mechanism;
- Eley–Rideal (E-R) mechanism.

(a) In the MVK mechanism, as shown in Fig. 27a, the VOC molecules react with the lattice oxygen on the catalyst surface to form the oxygen vacancies on the catalyst surface. Then, the reduced center was created by removing gaseous oxygen or

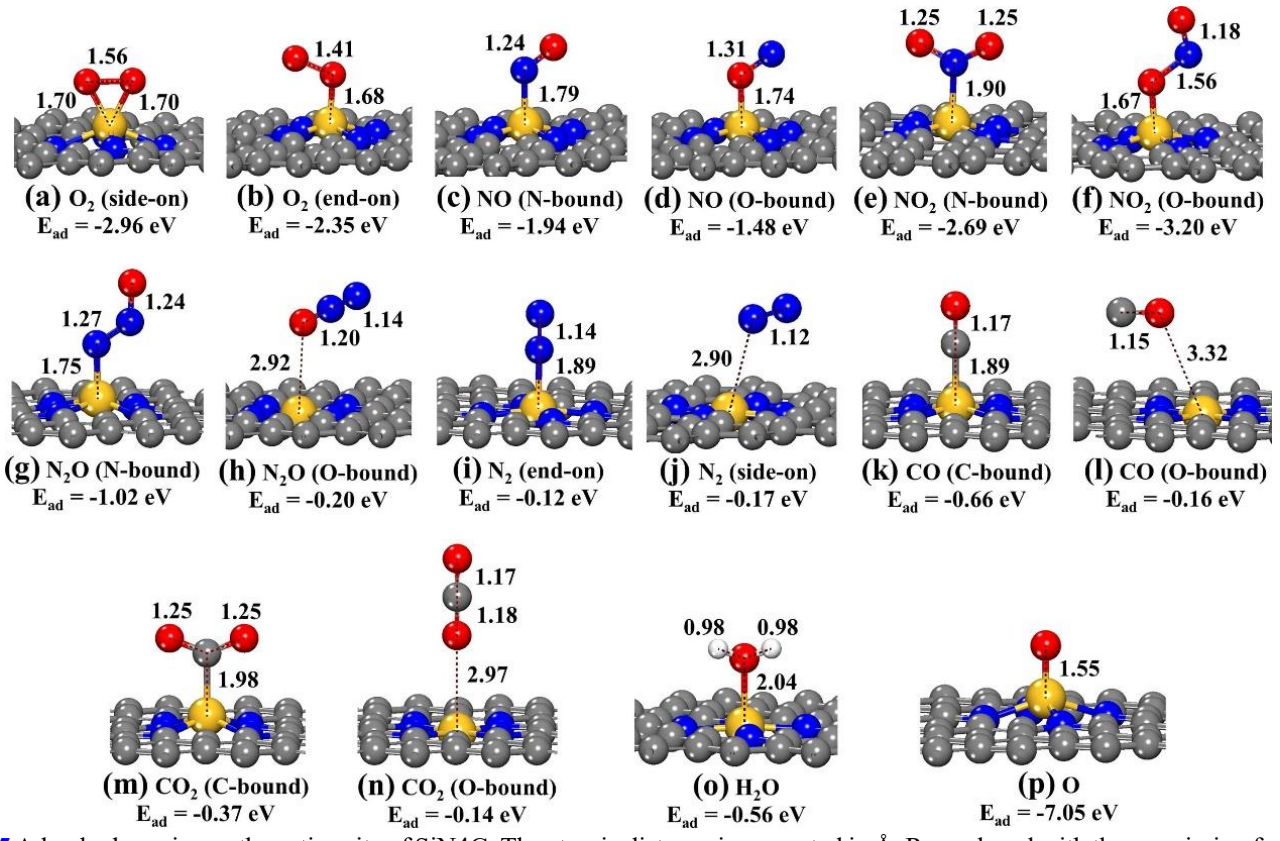

Fig. 25 Adsorbed species on the active site of SiN4G. The atomic distance is presented in Å. Reproduced with the permission from[120], Copyright 2020 Elsevier B. V.

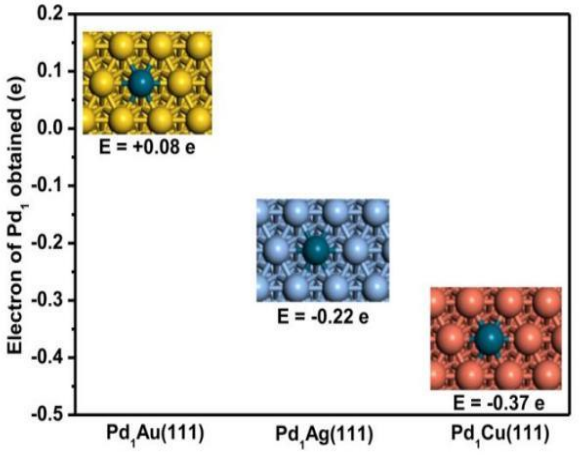

Fig. 26 DFT calculation results of electron states of isolated Pd atoms on alloying into Au (111), Ag (111), and Cu (111) surfaces. Reproduced with the permission from[121], Copyright 2017 American Chemical Society.

oxygen atoms from the bulk.[122,125]

(b) In the L-H mechanism, as shown in Fig. 27b, the first step of the L-H mechanism is the oxygen and VOCs adsorption on the catalyst, followed by the redox process. Whether VOCs and oxygen adsorb on the same active sites, the L-H model can be divided into a single site L-H model and a dual-site L-H model.[126,128]

(c) The E-R mechanism is demonstrated in Fig. 27c; the VOCs are oxidized in the gas phase with oxygen atoms adsorbed on the catalyst surface.[129, 130]

Wu *et al.* performed DFT calculation to study the reduction of N_2O on CaS (100) surface,[132] to analyze the sulphur effect, N_2 selectivity,[133] and N_2O decomposition products on the CaO surface,[134] later studied the mechanism of SO_x removal on N_2O emission in CFB boiler.[135] The findings proposed the reaction N_2O reduction pathway on the CaS (100) surface, displayed sulphur effects on the CaO deactivation, selectivity for N_2O decomposition, and the SO_x intermediate pathway (Fig. 28).

4.2.2 Mechanism of selective conversion

Fe and Cr doped (photocatalyst) on TiO_2 for the benzene oxidation to phenol were studied under ambient conditions and solar illumination source and ultraviolet (UV) irradiation.[136] Incorporated Fe and Cr ($Ti_{0.98}Fe_{0.02}O_2$) ($Ti_{0.98}Fe_{0.01}Cr_{0.01}O_2$) exhibited excellent catalytic activity and oxidation for benzene-to-phenol oxidation, which was attributed to the introduction of the Fe and Cr dopant into the TiO_2 structure. The conversion mechanism is shown in Fig. 29 below.

NO reduction and N_2O formation mechanisms over Mn/SBA-15 and Fe-Mn/SBA-15 were investigated through in situ DRIFT studies and a quick reaction study (Fig. 30). The characteristic of the Fe-Mn/SBA-15 catalyst in terms of low acidity, high basicity, and strong oxidation contributed to the nitrate production during the reaction. The nitrate produced decreases the N_2 selectivity due to the N_2O formation. The

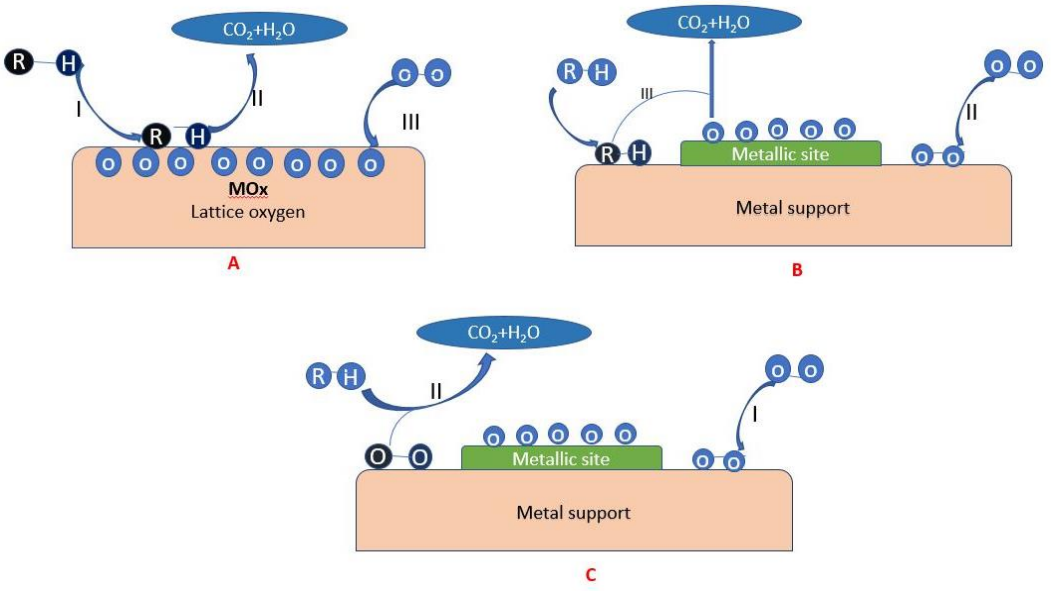

Fig. 27 Schematic diagrams of (a) MVK mechanism; (b) L-H mechanism; (c) E-R mechanism. Reproduced with the permission from[131], Copyright 2019 Elsevier B.V.

mechanism of de-nitration on the Fe-Mn/SBA-15 catalyst followed Langmuir−Hinshelwood, Eley−Rideal, and Mars−van Krevelen mechanisms.[137]

4.2.3 Mechanism of dry reforming

For Ni/La_2O_3 catalysts, CH_4 activation and dissociation occur on the Ni particle's surface to produce H_2 and active carbon intermediate species. The adsorption of CO_2 on La_2O_3 to form $La_2O_2CO_3$ can react with adjacent carbonaceous intermediate species to produce CO and regenerate La_2O_3. (Fig. 31). In this, $La_2O_2CO_3$ is used as an indicator to reflect the degree of active metal dispersion on La_2O_3 support. Good metal dispersion, $La_2O_2CO_3$ eliminated coke.[138]

4.2.4 Mechanism of Fischer-Tropsch synthesis

Recently, Buchang Shi *et al.* studied the inverse isotope effect and deuterium enrichments in hydrocarbons in Fe catalyzed Fischer-Tropsch reaction.[139] They explained their result by an Alkylidene mechanism in which the building block (monomers) of the polymerization reaction is M ≡ CH. The growing chain is RCH = M. The formation of the C − C bond is through the reaction of M ≡ CH and RCH = M, producing a new growing chain RCH_2CH = M (see Fig. 32). Detained calculations based on the alkylidene mechanism predict the deuterium enrichment, the function of carbon number.

5. Applications

Recently, a substantial number of research publications have been published in total conversion, selective NOx conversion, methane reforming (dry and steam reforming), FTs, and VOC oxidation, as illustrated in Fig 33. The charts showed a high amount of research works on methane reforming compared with other catalytic applications. Moreover, research on VOC oxidation shows a steady increase yearly as we can see that the number of publications considerably increased in 2021.

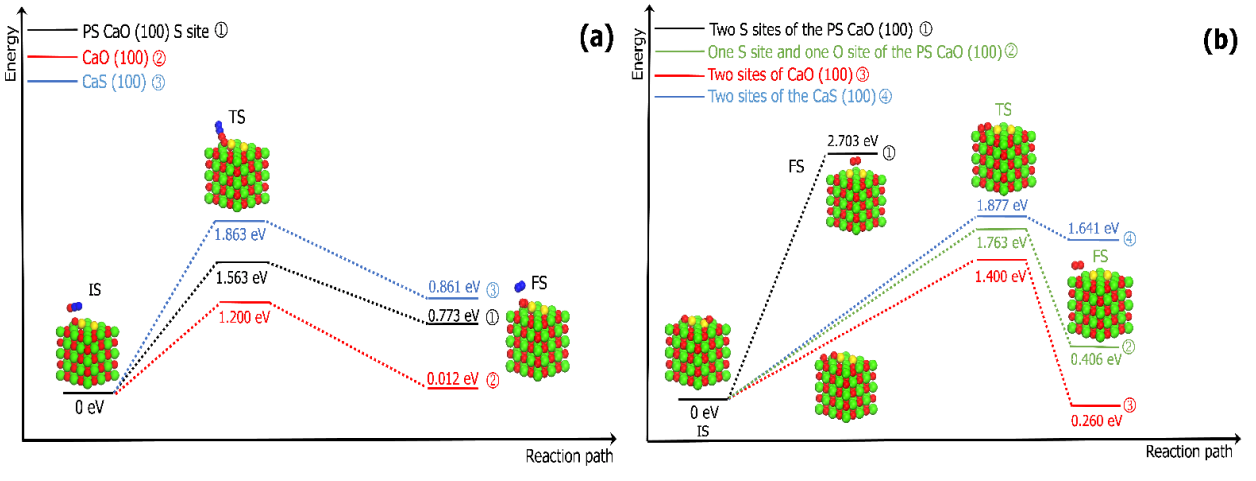

Fig. 28 The ER route for CaO surface recovery (a) and LH route for CaO surface recovery (b). reproduced with the permission from[135], Copyright, 2015 Elsevier B.V.

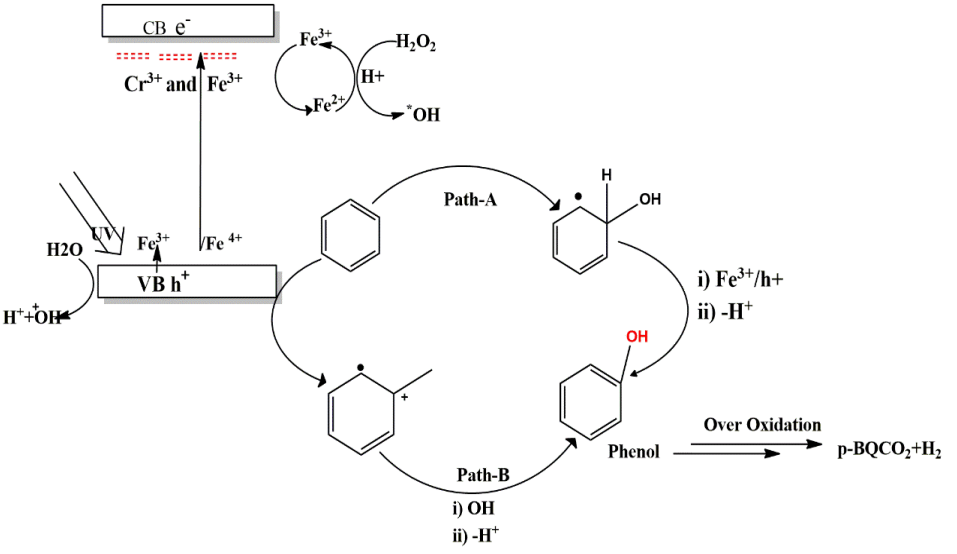

Fig. 29 proposed the mechanism of photocatalytic benzene oxidation to phenol. Reproduced with the permission from[136], Copyright 2018 Elsevier B.V.

5.1 Complete VOCs abatement

Catalytic oxidation of VOCs is a preferable method of reducing/abating VOCs at moderate temperature into harmless CO_2 and H_2O, compared to thermal incineration, which is expensive and requires a substantial energy input to destroy dilute gas phase containing VOCs at relatively high temperature (750 °C) and at the same time produce toxic by-products to the environment.

Recently, transition metal oxides catalysts have received increased attention in VOCs total abatement because of their superior thermal stability and lower cost than noble metal oxides, whose use is restricted due to their low stability, high cost, and proclivity for poisoning. Therefore, performance toward abatement of VOCs with TMOs can even compete with Noble metals due to the aforementioned properties. Several TMOs show highly effective catalysts consisting of single, binary and mixed oxides, such as manganese and cobalt oxides,[32-84-140-144] cerium based oxides,[9,145] copper-based oxides[32-146-148] lanthanum based oxides and lanthanum-based perovskites,[75-149-150] zeolite as catalyst and support[151,153] has been studied for VOCs abatement, and their results show high potential activity for CO and VOCs oxidation. Fig. 34 shows some selected catalysts that have been applied for VOCs' complete abatement.

5.2 Selective conversion in NO_x reduction

Selective catalytic reduction with NH_3 (NH_3-SCR) is an efficient method for the reduction of NO_x in cars and industries. However, during SCR reactions, catalysts were deactivated by sulphur poisoning, water, and alkaline poisoning, especially at low-temperature operation, shifting the researcher's attention toward low-temperature SCR with operational temperature below 250 °C. Therefore, resistance to H_2O effects, SO_2, and alkali poisoning at low temperatures have to be fulfilled to avoid damage to the morphology and structure of catalysts, leading to the deactivation of catalysts.

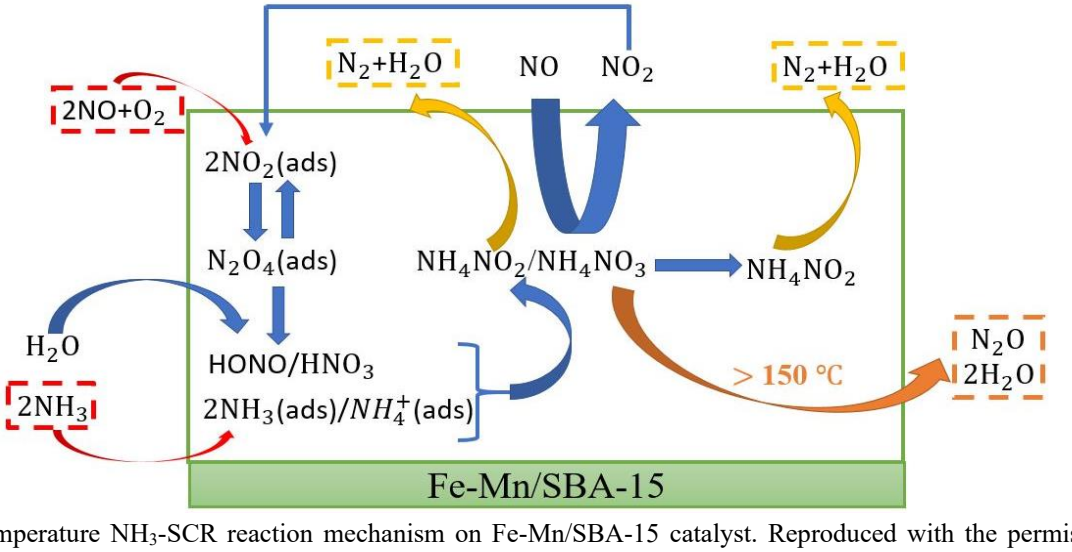

Fig. 30 Low-temperature NH_3-SCR reaction mechanism on Fe-Mn/SBA-15 catalyst. Reproduced with the permission from[137], Copyright 2018 American Chemical Society.

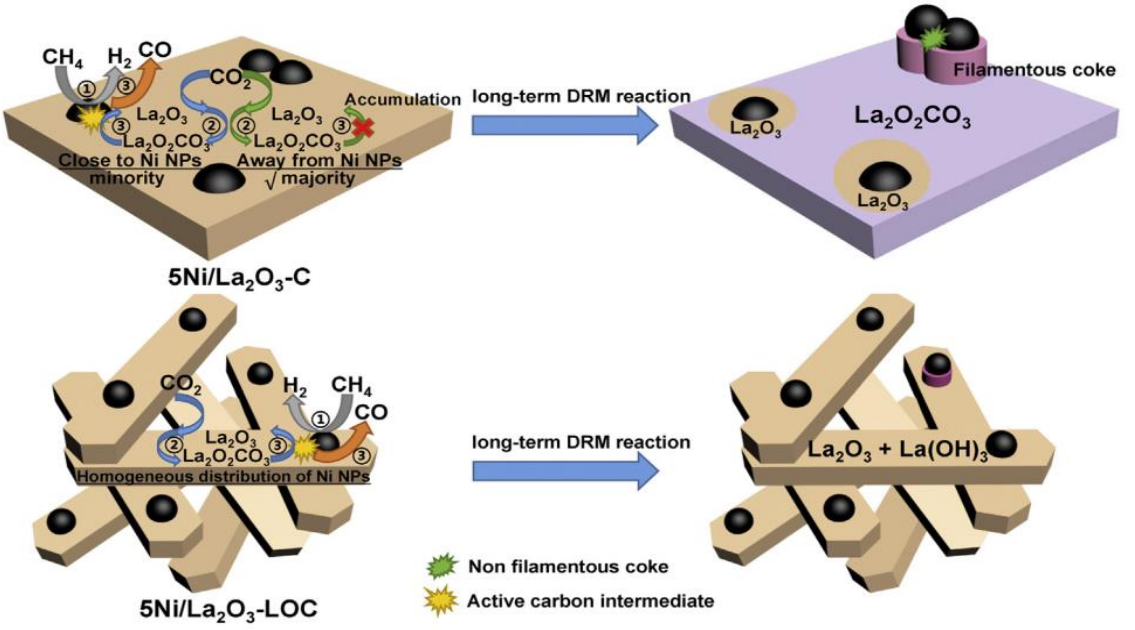

Fig. 31 Scheme of the catalyst models and reaction mechanisms in the DRM process. Reproduced with the permission from[138], Copyright 2019 Elsevier B.V.

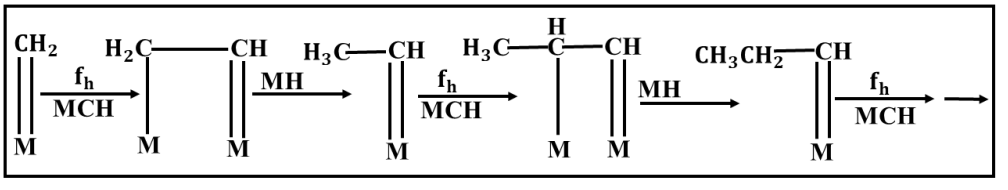

Fig. 32 Alkylidene Mechanism for Fe catalyzed Fischer-Tropsch Synthesis (A) CO/H_2 as the syngas. Reproduced with the permission from [138], Copyright 2019 Elsevier B.V.

Recently, Guo *et al.* developed a highly efficient and poison-resistant SCR catalyst via improving Mn-Eu catalyst with Fe. The catalyst maintained a high performance toward NO conversion and H_2O resistance at low temperatures. This was attributed to the strong relationship among Mn, Eu, and Fe.[154] Jiang Haoxin *et al.*[155] also control the morphology of manganese oxides (MnO_x) catalyst via the solvent-thermal method for low-temperature selective NOx conversion by revealing crystal faces of a-MnO_2 nanorods. The exposed facets were found to impact catalyst activities significantly.

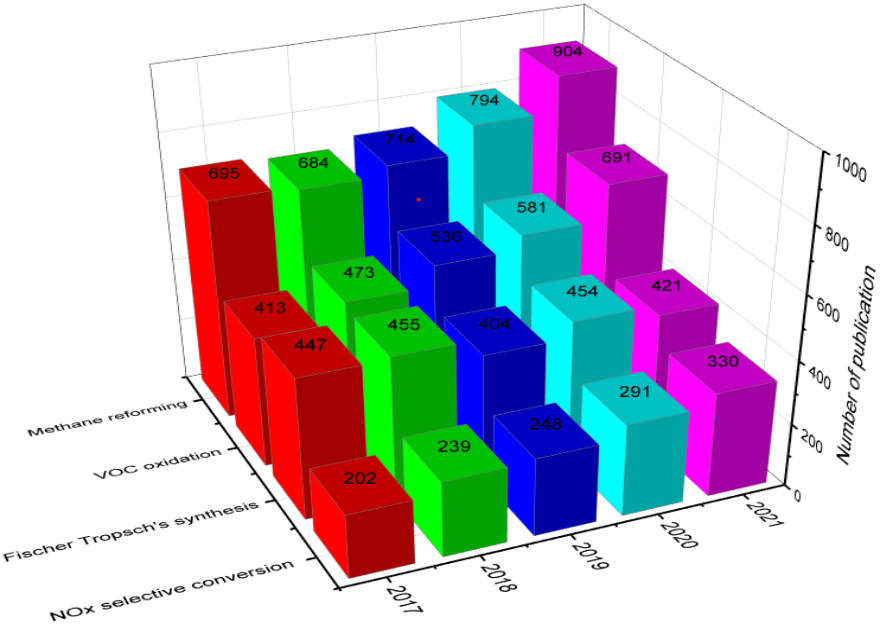

Fig. 33 Number of publications on some selected catalytic applications for four years.

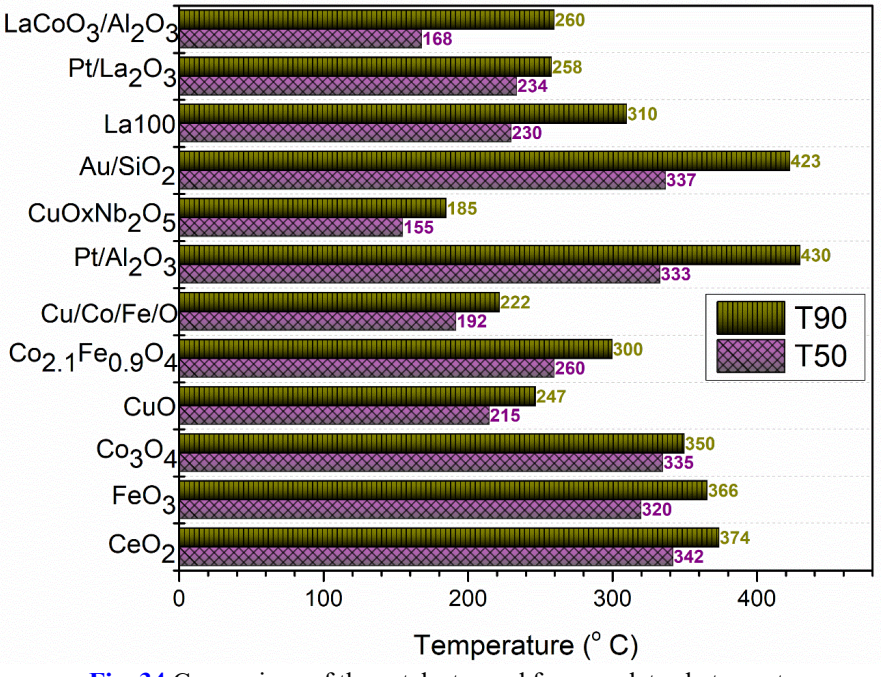

Fig. 34 Comparison of the catalysts used for complete abatement.

The investigation of the metal poisoning toward NH_3-SCR and the resistances of Cu-SSZ-13 to hydrothermal aging and alkali metal poisoning for selective catalytic reduction of NO_x with NH_3 was investigated, and the result revealed that the alkali metal loading of up to 0.50 mmol/g_{cat} exhibited the highest resistance to alkali metal poisoning[156] (see Fig. 35).

Li *et al.* doped Lanthanide perovskite catalysts with limited palladium and cerium using the sol-gel method to improve activity and sulphur resistance. In different B sites, lanthanide perovskites were studied for H_2 selective catalytic reduction of NO. The activity sequence was found to follow this sequence: LaCeMnPd > LaCeCoPd > LaCeFePd. LaCeMnPd has a high NO conversion of 96.6% at only 150 °C. and high SO_2 resistance in different SO_2 concentrations.[157]

Yamamoto *et al.* also investigated the effect of SO_2 gas over a TiO_2 photocatalyst in the presence of excess oxygen (photo-SCR). The induced SO_2 at 300 ppm decreased the activity of the photo-SCR at 373 K. And, consequently, it increased the reaction temperature, favor the resistance to SO_2 and the catalyst activity toward NOx reduction.[158] A review by Han *et al*. summarised the deactivation effects, deactivation process, and the possible solution.[38] Fig. 36 resumes the deactivation processes caused by sulphur oxides (SO_x).

5.3 Propane-propene/alkenes/alcohols

The process of catalytic dehydrogenation of propane into propene (ODHP) has attracted attention because propene constitutes an essential class of intermediates in the petrochemical industry. Due to the rapidly increasing demand for propene, oxidative dehydrogenation of propane has become a new route of propene production. However, this process suffers from a significant loss of propane selectivity

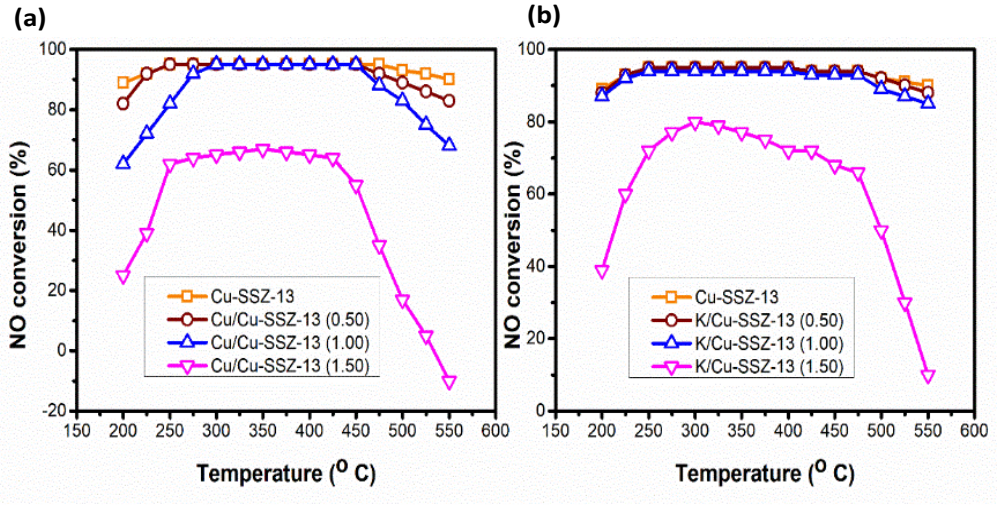

Fig. 35 NH_3-SCR performances of the fresh and alkali metal poisoned Cu-SSZ-13 catalysts. Reproduced with the permission form[156], Copyright 2017 Elsevier B.V.

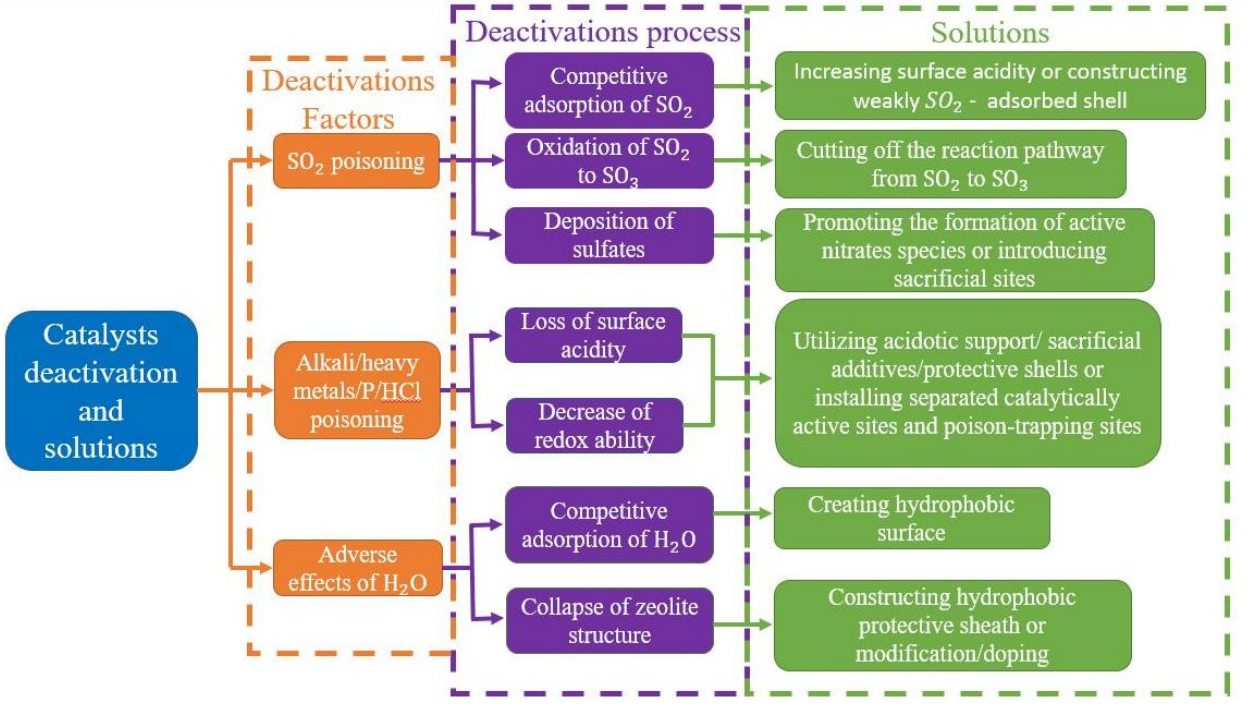

Fig. 36 Deactivation processes caused by SO_x, alkali/heavy metal/P/HCl, or H_2O and the corresponding strategies for improving the poisoning resistance and hydrothermal stability. Reproduced with the permission form[159], 2019 American Chemical Society.

due to the over-oxidation of propane to carbon dioxide in the reaction. Many attempts were made toward addressing these drawbacks by replacing oxygen with soft oxidants, such as N_2O and CO_2. Among the catalyst used for propane dehydrogenation, Ga_2O_3 and Cr_2O_3-based catalysts proved to be more active and efficient for ODHP reaction.[160,165] They are also used to improve other catalyst materials' catalytic performance.[166,175] Fig. 37 provides the tendency of some selected catalysts used to convert propane to propene.

5.4 Dry Reforming

Catalytic dry reforming of methane (DRM) is an effective and potential process to utilize CH_4 and CO_2 to produce a mixture of CO and H_2 (syngas). As shown below, carbon dioxide is used as the oxidant instead of water as in steam reforming.

$$CH_4 + CO_2 \leftrightarrow 2CO + 2H_2 \quad (2)$$

The Syngas produced during the reaction above can be used as a feedstock for the Fischer–Tropsch synthesis to convert cleaner fuels, such as gasoline, methanol, dimethyl ether (DME), and gasoline.

During dry reforming, there are many side reactions aside from water reverse water-gas shift (RWGS) reaction, like decomposition of methane and disproportionation reaction leading to catalyst deactivation at high temperature (eq. 4 & 5)

$$H_2 + CO_2 \leftrightarrow H_2O + CO \text{ reverse water-gas – shift (RWGS)} \quad (3)$$

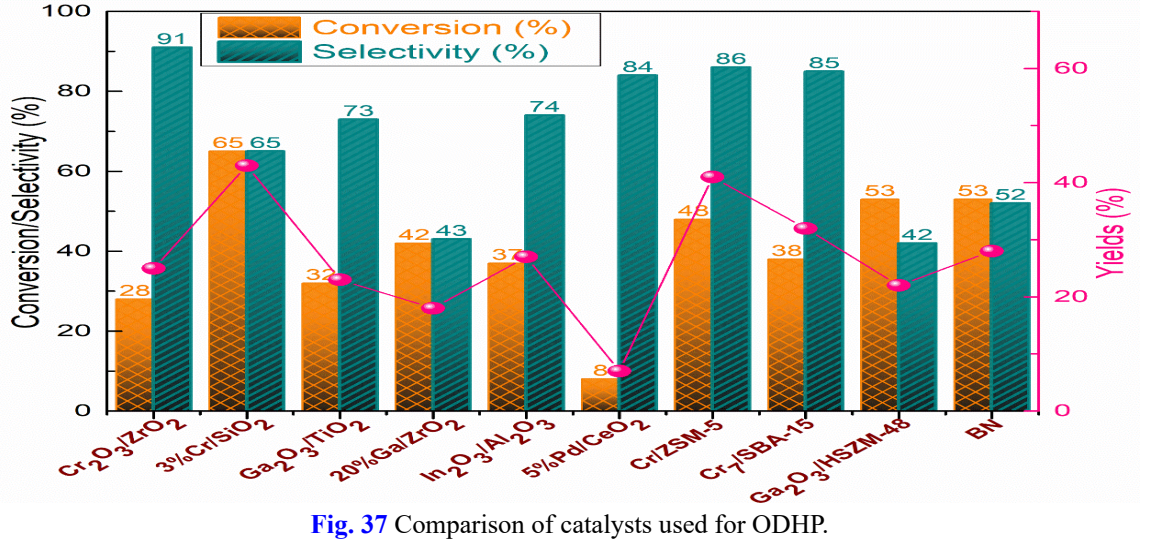

Fig. 37 Comparison of catalysts used for ODHP.

Note: SBA refers to mesoporous silica materials; BN refers to Boron-Nitride; ZSM-5 and HZSM-48 refer to Zeolite Socony Mobil 5 and 48, respectively.

$$CH_4 \leftrightarrow 2H_2 + C \text{ methane cracking/decomposition} \quad (4)$$

$$2CO \leftrightarrow C + CO_2 \text{ Boudouard or CO disproportionation} \quad (5)$$

Therefore, to prevent the side reaction and to improve the DRM reaction, the choice of a catalyst with high resistance to carbon formation, improved stability, increased activity, and selectivity is essential. Zhang *et al.* reported that the high alkalinity of the supported catalyst on metal oxide (MO) prevents carbon deposition during DRM.[176] Li *et al.* also reported that Ru supported Mg-Al Oxides for DRM, revealing high catalytic, which could be linked to the strong basicity of the support with more available Ru surface atoms.[177] Hence, these lead to a significant number of researches on the the use of metals as primary support for reforming CH_4 with CO_2.

Therefore, a better alternative to reduce the acidity in support is to use basic metal oxides to serve as adequate support, *e.g.* alkaline earth metal oxides.[178] According to the literature, transition metals such as Ni, Fe, Co, and Mn are more generally utilized as active metals in dry methane reforming than noble metals due to their low cost and availability. The promotion of a catalyst plays a vital role in reducing carbon deposition and improving dry reforming.[179] Gd-promoted Ni/Y_2O_3 catalyst has been reported to be active at high temperatures and to reduce the carbon deposition due to the dissociative adsorption of methane, which is associated to the basicity of the catalyst.[180]

Since dry reforming (CO_2 reforming of CH_4) reaction operates at high temperatures, perovskite oxides (ABO_3) could have an advantage since they are resistant to high thermal stability and carbon resistance.[181] *e.g.*, single-phase $La_{1-x}Ba_xMnO_3$ perovskite catalyst shows high activity and selectivity toward CH_4 and CO_2 conversions with much-reduced coke formation even at high temperatures by replacing La^{3+} by Br in $LaMnO_3$ as single-phase $La_{1-x}Ba_xMnO_3$ perovskite.

5.5 Fischer-Tropsch

The Fischer-Tropsch synthesis is a polymerization technique that converts carbon sources into hydrocarbons chains (gas to liquid fuel) through the hydrogenation of carbon monoxide in the presence of a metal catalyst, as shown below. The carbon sources can be obtained through the gasification of coal and natural gas reforming.[182,183]

$$CO + 2H_2 \rightarrow [CH_2] + H_2O \; \Delta H = -167,4 \text{ kJ/mole CO} \quad (6)$$

where $[CH_2]$ is the monomer of the hydrocarbon molecules. Fischer-Tropsch reaction is a highly exothermic process that leads to catalyst deactivation via the Boudouard reaction. Therefore, excess heat needs to be reduced from this process.[182]

5.5.1 Fischer Tropsch catalyst

Since Fischer and Tropsch discovered gasoline synthesis in 1926, Iron and cobalt have been used as catalysts in this process.[184] The most widely used catalyst are Iron, Cobalt, Ruthenium, and Nickel to polymerize syngas into hydrocarbon chains in this reaction pattern:

$$nCO + (2n+1)\, H_2 \rightarrow C_nH_{2n+2} + nH_2O \quad (7)$$

During the reaction process, high temperature, sulphur contamination, and the presence of water contribute to the catalyst's deactivation. For example, Iron is more susceptible to carbon cobalt and is more vulnerable to sulphur poisoning.[184]

So, Iron is a better choice for CO-rich syngas such as coal or biomass and similarly a poor choice for H-rich syngas from natural gas due to its high resistance towards sulphur poisoning, and low selectivity of methane, high selectivity to WGS (water gas shift) activity, and low cost of Fe.[185] While cobalt-based FTs catalysts have advantages of superior catalyst stability, high yield towards linear hydrocarbons, low operating temperature, and low WGS activity.[186]

5.5.2 Effects of water on FT synthesis

The water influence on FT synthesis is of significant importance, particularly on cobalt, due to partial exhibiting of WGS activity and increasing the CO conversion and residence time and the partial water pressure. The water effect on cobalt catalysts for CO conversion is still debated. Several researchers investigated the impact and came up with results ranging from negative[187] to negligible[188] to even positive effect,[189] depending on the support and dispersion of the supported metal, which is controlled by the loading, preparation method, and pre-treatment process.

On the other hand, iron-based catalysts exhibit higher selectivity to intrinsic water-gas shifts due to their ability to convert syngas with a lower H_2/CO ratio, especially those derived from coal gasification. While cobalt catalysts display little effect on the water-gas-shift reaction. These controversies lead to more research on the impact of water on the activity, selectivity, and stability of cobalt catalysts and the chemical and structural changes of the catalyst.

Davis *et al*.[189] reported that water negatively affected the CO conversion on Co/TiO_2 and Pt promoted Co/Al_2O_3 catalysts. Bertole *et al*. investigated the effect of water on the cobalt catalyst for Fischer–Tropsch synthesis. They found that water co-feeding had a negligible impact on CO conversion even at a few bars of syngas pressures.

A study on the effect of water on FTs over supported cobalt catalysts by Storsæter *et al*. reported that the water effect on the selectivity and activity show a different behavior, according to the type of support: For the Al_2O_3-supported catalysts, the activity was almost unchanged as the conversion was increased, whereas the addition of external water deactivated the catalysts. The deactivation observed was more significant at higher water partial pressures and only partly reversible after removing the water. The addition of water resulted in more significant deactivation for the Re-promoted catalyst.[190]

Pendyala *et al*.[191] investigated the effect of water on the performance of potassium promoted iron catalyst for FTs using a continuously stirred tank reactor (CSTR) at two

different reaction temperatures; they observed that the water whereas for the reaction carried out at 230°C the added water decreased CO conversion and deactivated the catalyst. It was concluded that the addition of water at 230°C oxidized the catalyst by transforming the iron carbide into the Fe_3O_4 phase. But severe oxidization did not occur as the carbide phase was retained at 270 °C. The loss inactivity and deactivation rate were more pronounced at 230°C compared to the 270 °C conditions for the same catalyst. The effect of water on CO conversion for potassium promoted iron catalyst carried out at 230°C is shown in Figs. 38(a) and 38(b).

5.5.3 Effect of support, promoters, and loading on FTs catalyst

Catalytic modifiers or promoters can influence the activity or the selectivity of catalysts, either through structural modification, chemical or electrostatic interaction with the catalytically active material. Roh H. *et al.* [192] reported a study on the effect of zirconia loading on alumina-supported cobalt promoted for FTs-catalysts; the catalysts show higher activities and improved selectivity to higher hydrocarbons in CO hydrogenation with the increase in zirconia loading.

A doped Co–Re/γ-Al_2O_3 catalyst was impregnated with alkaline earth elements (Li, Na, K, and Ca) ranging from 25 to 20 000-ppm. The results revealed that adding alkaline earth metals of up to 1000 ppm to Co–Re/γ-Al_2O_3 catalyst has no effect on H_2 chemisorption but rather reduces the site yields.[193] Miller *et al*. also obtained similar results while evaluating the impact of pre-treatment of potassium addition on supported iron catalysts for the Fischer-Tropsch reaction (Fig. 39).[194]

added has a positive effect on CO conversion at 270°C

The effects of [Fe]/[Mn] molar ratios, promoters, loading of the optimal promoter, and calcination conditions on the catalytic performance of iron–manganese catalysts for the FTs were investigated. It was found that the 50%Fe/50%Mn catalyst was promoted with 6 wt.% K is an optimal catalyst for converting synthesis gas to hydrocarbons, exceptionally light olefins.[195]

Supported cobalt is considered the most favorable catalytic material for synthesizing long-chain hydrocarbons from natural gas-based synthesis gas because of its high activity, high selectivity for linear paraffin, and low water-gas shift activity, and low price compared to noble metals. The Commonly used supports for Fischer-Tropsch catalysts include alumina, silica, and Titania.[196] It has been observed that the promotion of alumina-supported Co-containing catalysts by adding specific amounts of Pt leads to an increase in the formation of high molecular-weight hydrocarbons.[197] Effects of Mo loading and carbons on activity, stability, and selectivity to hydrocarbons and alcohols during FTs over Fe-Mo-Cu-K/AC catalysts also reveal that Mo promoter improves catalyst stability, which may be attributed to Mo inhibiting iron particle agglomeration during the FTs reaction.[198]

The addition of small amounts of rhenium to a 15% Co/Al_2O_3 catalyst decreased cobalt oxide's reduction temperature. Still, there is no significant change in the percentage dispersion and cluster size based on the quantity of reduced cobalt.[199] The addition of rhenium increases the percentage reduction of cobalt and increases the initial activity, as shown in Fig. 40.

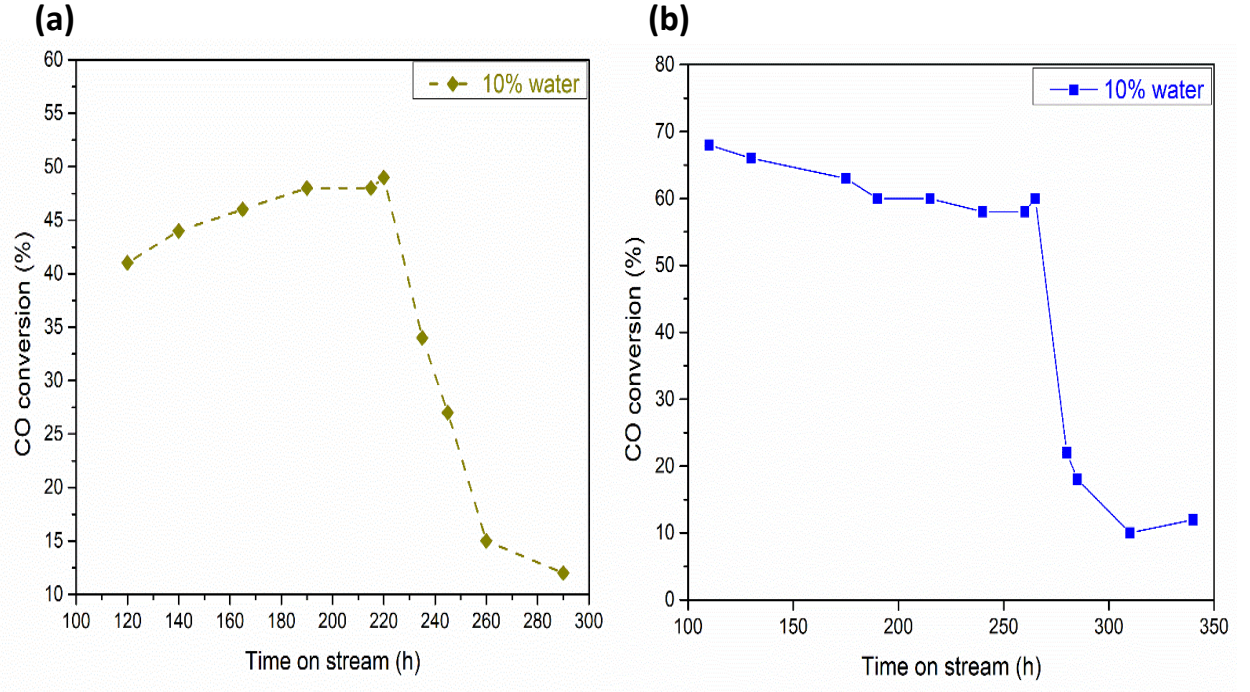

Fig. 38 (a) Effect of water on CO conversion for potassium promoted iron catalyst at 230 °C (T=230 °C P = 13 atm (1.31 MPa), H_2/CO= 0.7, SV = 6 SL/g Fe/h). (b)Effect of water on CO conversion for potassium promoted iron catalyst at higher conversion level. (T=230 °C, P = 13 atm (1.31 MPa), H_2/CO= 0.7, SV = 2 SL/g Fe/h). Reproduced with the permission form[191], Copyright 2010, Springer Science Business Media, LLC.

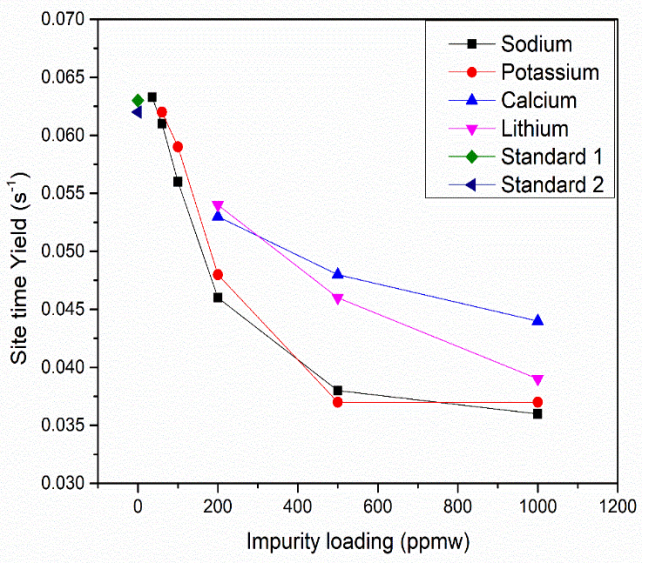

Fig. 39 Site time yield plotted against mol impurities/Co surface sites for all catalysts containing 1000 ppm or less impurity. Reproduced with the permission form[193], Copyright 2013 Elsevier B. V.

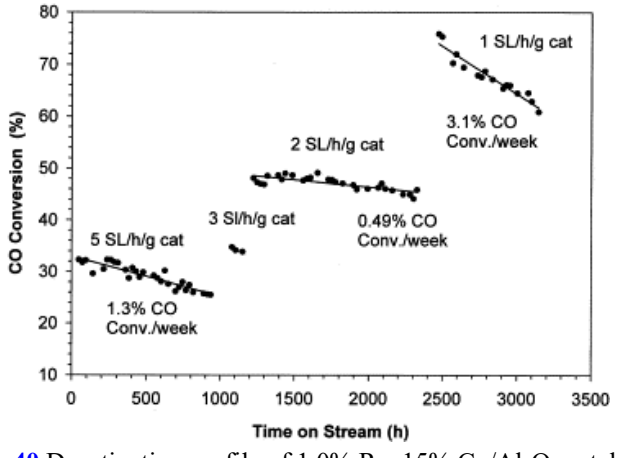

Fig. 40 Deactivation profile of 1.0% Re–15% Co/Al_2O_3 catalyst, temperature=493 K, pressure=19.7 atm, H_2/CO=2:1, start-up solvent=Polywax-3000. Reproduced with the permission form[199], Copyright 2002 Elsevier Science Ltd.

6. Conclusion and perspectives

Catalysis is the process that transforms chemical species into other products by altering the pathway to increase the yield using selective catalysts. It is a technique utilized by several petrochemical industries to increase/decrease the production process and environmental pollutant control, such as VOCs and NO_x, at low temperatures. This review paper provides a comprehensive overview of catalyst preparation, characterization, and application to complete abatement of VOCs, selective conversion, FTs, and methane reforming. Several preparation techniques for catalysts such as impregnation, precipitation/co-precipitation, sol-gel, PSE-CVD, hydrothermal, and flame spray pyrolysis to synthesize noble metal oxides, transition metal oxides, a single atom, perovskite, and zeolite have been reviewed in this work. Various characterization techniques were highlighted to identify the crystalline phases, morphology, microstructure, chemical composition, surface area, structure stability, and the pore structure of different catalysts. The details on how water affects catalytic performance, sulphur poisoning, alkali poisoning, and the success of overcoming such drawbacks have been discussed. Despite many studies on catalyst preparations methods, characterization techniques, and applications of catalysts, more future research strategies are expected toward:

(a) The enrichment of the catalyst family with new synthesis and characterization techniques like Helium ion microscopy (HIM) and Electron energy loss spectroscopy (EELS).
(b) Designing more stable, selective, and cost-effective catalysts will efficiently remove a significant number of VOCs.
(c) Developing highly active transition metal oxides catalysts for VOC oxidation at low temperature.
(d) Effect of water vapor adsorption on the catalyst surface at low temperature.
(e) The mixture of VOCs with SO_x and NO_x to simulate the absolute VOC emission control.
(f) MnO_x as catalyst support for FT synthesis and methane reforming due to sulphur and water-resistant effect.
(g) Synthesis of single-atom catalysts for Fischer-Tropsch synthesis and steam methane reforming.
(h) Studies on the conversion of low-cost industrial by-products to high demand chemical products like dehydrogenation of ethane to ethylene and propane to propene
(i) Studies on reaction route control to reduce secondary reaction intermediate to achieve the desired product.

Acknowledgement

The authors thank for the financial support from the National Natural Science Foundation of China (No. 51888103/51976216/52161145105/M-019), the Ministry of Science and Technology of China (2021YFA0716204/2017YFA0402800), Beijing Municipal Natural Science Foundation (JQ20017), K.C. Wong Education Foundation (GJTD-2020-07) and National Science and Technology Major Project (J2019-III-0005-0048).

Conflict of Interest

The authors declare no conflict of interest.

Supporting information

Not applicable.

References

[1] M. Han, X. Lu, C. Zhao, L. Ran, S. Han, Characterization and source apportionment of volatile organic compounds in urban and suburban Tianjin, China, *Advances in Atmospheric Sciences*, 2015, **32**, 439-444, doi: 10.1007/s00376-014-4077-4.

[2] S. A. C. Carabineiro, M. Konsolakis, G. E.-N. Marnellos, M. F. Asad, O. S. G. P. Soares, P. B. Tavares, M. F. Ribeiro Pereira, J. J. de Melo Orfao, J. L. Figueiredo, Ethyl acetate abatement on copper catalysts supported on ceria doped with rare earth oxides, *Molecules*, 2016, **21**, doi: 10.3390/molecules21050644.
[3] J. Li, W. Li, Effect of preparation method on the catalytic activity of Au/CeO_2 for VOCs oxidation, *Journal of Rare Earths*, 2010, **28**, 547-551, doi: 10.1016/s1002-0721(09)60151-4.
[4] Y. Y. Broza, R. Vishinkin, O. Barash, M. K. Nakhleh, H. Haick, Synergy between nanomaterials and volatile organic compounds for non-invasive medical evaluation, *Chemical Society Reviews*, 2018, **47**, 4781-4859, doi: 10.1039/c8cs00317c.
[5] M. Mao, Y. Li, H. Lv, J. Hou, M. Zeng, L. Ren, H. Huang, X. Zhao, Efficient UV-vis-IR light-driven thermocatalytic purification of benzene on a Pt/CeO_2 nanocomposite significantly promoted by hot electron-induced photoactivation, *Environmental Science: Nano*, 2017, **4**, 373-384, doi: 10.1039/c6en00472e.
[6] R. Dardouri, R. M. Navarro Yerga, N. Mota, B. Albela, L. Bonneviot, M. S. Zina, Lower methane combustion temperature on palladium nanoparticles anchored on TiO_x subnano-islets in stellate mesoporous silica nanospheres, *New Journal of Chemistry*, 2020, **44**, 906-919, doi: 10.1039/c9nj04554f.
[7] S. Tian, B. Wang, W. Gong, Z. He, Q. Xu, W. Chen, Q. Zhang, Y. Zhu, J. Yang, Q. Fu, Dual-atom Pt heterogeneous catalyst with excellent catalytic performances for the selective hydrogenation and epoxidation, *Nature communications*, 2021, **12**, 1-9, doi: 10.1038/s41467-021-23517-x.
[8] J. Fernández-Catalá, G. Garrigós-Pastor, Berenguer-Murcia, D. Cazorla-Amorós, Photo-microfluidic chip reactors for propene complete oxidation with TiO_2 photocalyst using UV-LED light, *Journal of Environmental Chemical Engineering*, 2019, **7**, 103408, doi: 10.1016/j.jece.2019.103408.
[9] J. I. Gutiérrez-Ortiz, B. de Rivas, R. López-Fonseca, J. R. González-Velasco, Combustion of aliphatic C2 chlorohydrocarbons over ceria-zirconia mixed oxides catalysts, *Applied Catalysis A: General*, 2004, **269**, 147-155, doi: 10.1016/j.apcata.2004.04.014.
[10] S. Lee, A. Halder, G. A. Ferguson, S. Seifert, R. E. Winans, D. Teschner, R. Schlögl, V. Papaefthimiou, J. Greeley, L. A. Curtiss, S. Vajda, Subnanometer cobalt oxide clusters as selective low temperature oxidative dehydrogenation catalysts, *Nature Communications*, 2019, **10**, 954, doi: 10.1038/s41467-019-08819-5.
[11] Y. Inomata, H. Kubota, S. Hata, E. Kiyonaga, K. Morita, K. Yoshida, N. Sakaguchi, T. Toyao, K.-I. Shimizu, S. Ishikawa, W. Ueda, M. Haruta, T. Murayama, Bulk tungsten-substituted vanadium oxide for low-temperature NO_x removal in the presence of water, *Nature Communications*, 2021, **12**, 557, doi: 10.1038/s41467-020-20867-w.
[12] M. Akri, S. Zhao, X. Li, K. Zang, A. F. Lee, M. A. Isaacs, W. Xi, Y. Gangarajula, J. Luo, Y. Ren, Y. T. Cui, L. Li, Y. Su, X. Pan, K. Wilson, L. Li, B. Qiao, H. Ishii, Y. F. Liao, A. Wang, X. Wang, T. Zhang, Atomically dispersed nickel as coke-resistant active sites for methane dry reforming, *Nature Communications*, 2019, **10**, 5181, doi: 10.1038/s41467-019-12843-w.
[13] M. R. Goldwasser, M. E. Rivas, E. Pietri, M. J. Pérez-Zurita, M. L. Cubeiro, A. Grivobal-Constant, G. Leclercq, Perovskites as catalysts precursors: synthesis and characterization, *Journal of Molecular Catalysis A: Chemical*, 2005, **228**, 325-331, doi: 10.1016/j.molcata.2004.09.030.
[14] P. Esmaeilnejad-Ahranjani, A. A. Khodadadi, Y. Mortazavi, Self-regenerative function of Cu in $LaMnCu_{0.1}O_3$ catalyst: towards noble metal-free intelligent perovskites for automotive exhaust gas treatment, *Applied Catalysis A: General*, 2020, **602**, 117702, doi: 10.1016/j.apcata.2020.117702.
[15] S. Royer, D. Duprez, F. Can, X. Courtois, C. Batiot-Dupeyrat, S. Laassiri, H. Alamdari, Perovskites as substitutes of noble metals for heterogeneous catalysis: dream or reality, *Chemical Reviews*, 2014, **114**, 10292-10368, doi: 10.1021/cr500032a.
[16] C. Zhang, C. Wang, S. Gil, A. Boreave, L. Retailleau, Y. Guo, J. L. Valverde, A. Giroir-Fendler, Catalytic oxidation of 1, 2-dichloropropane over supported LaMnO oxides catalysts, *Applied Catalysis B: Environmental*, 2017, **201**, 552-560, doi: 10.1016/j.apcatb.2016.08.038.
[17] R. López-Fonseca, J. I. Gutiérrez-Ortiz, J. L. Ayastui, M. A. Gutiérrez-Ortiz, J. R. González-Velasco, Gas-phase catalytic combustion of chlorinated VOC binary mixtures, *Applied Catalysis B: Environmental*, 2003, **45**, 13-21, doi: 10.1016/s0926-3373(03)00106-1.
[18] I. Song, H. Lee, S. W. Jeon, I. A. M. Ibrahim, J. Kim, Y. Byun, D. J. Koh, J. W. Han, D. H. Kim, Simple physical mixing of zeolite prevents sulfur deactivation of vanadia catalysts for NO_x removal, *Nature Communications*, 2021, **12**, 901, doi: 10.1038/s41467-021-21228-x.
[19] D. Pan, F. Su, C. Liu, Z. Guo, Research progress for plastic waste management and manufacture of value-added products, *Advanced Composites and Hybrid Materials*, 2020, **3**, 443-461, doi: 10.1007/s42114-020-00190-0.
[20] P. Xie, T. Pu, A. Nie, S. Hwang, S. C. Purdy, W. Yu, D. Su, J. T. Miller, C. Wang, Nanoceria-supported single-atom platinum catalysts for direct methane conversion, *ACS Catalysis*, 2018, **8**, 4044-4048, doi: 10.1021/acscatal.8b00004.
[21] Z. Li, S. Ji, Y. Liu, X. Cao, S. Tian, Y. Chen, Z. Niu, Y. Li, Well-defined materials for heterogeneous catalysis: from nanoparticles to isolated single-atom sites, *Chemical Reviews*, 2020, **120**, 623-682, doi: 10.1021/acs.chemrev.9b00311.
[22] S. Ji, Y. Chen, X. Wang, Z. Zhang, D. Wang, Y. Li, Chemical synthesis of single atomic site catalysts, *Chemical Reviews*, 2020, **120**, 11900-11955, doi: 10.1021/acs.chemrev.9b00818.
[23] L. Zhang, M. Zhou, A. Wang, T. Zhang, Selective hydrogenation over supported metal catalysts: from nanoparticles to single atoms, *Chemical Reviews*, 2020, **120**, 683-733, doi: 10.1021/acs.chemrev.9b00230.
[24] D. Zhao, Z. Zhuang, X. Cao, C. Zhang, Q. Peng, C. Chen, Y. Li, Atomic site electrocatalysts for water splitting, oxygen reduction and selective oxidation, *Chemical Society Reviews*, 2020, **49**, 2215-2264, doi: 10.1039/c9cs00869a.
[25] Q. Ye, L. Wang, R. T. Yang, Activity, propene poisoning resistance and hydrothermal stability of copper exchanged

chabazite-like zeolite catalysts for SCR of NO with ammonia in comparison to Cu/ZSM-5, *Applied Catalysis A: General*, 2012, **427-428**, 24-34, doi: 10.1016/j.apcata.2012.03.026.
[26] U.-E.-S. Amjad, C. W. M. Quintero, G. Ercolino, C. Italiano, A. Vita, S. Specchia, Methane steam reforming on the Pt/CeO_2 catalyst: effect of daily start-up and shut-down on long-term stability of the catalyst, *Industrial & Engineering Chemistry Research*, 2019, **58**, 16395-16406, doi: 10.1021/acs.iecr.9b02436.
[27] C. Anil, J. M. Modak, G. Madras, Syngas production via CO_2 reforming of methane over noble metal (Ru, Pt, and Pd) doped $LaAlO_3$ perovskite catalyst, *Molecular Catalysis*, 2020, **484**, 110805, doi: 10.1016/j.mcat.2020.110805.
[28] S. Eriksson, S. Rojas, M. Boutonnet, J. L. G. Fierro, Effect of Ce-doping on Rh/ZrO_2 catalysts for partial oxidation of methane, *Applied Catalysis A: General*, 2007, **326**, 8-16, doi: 10.1016/j.apcata.2007.03.019
[29] N. Habibi, Y. Wang, H. Arandiyan, M. Rezaei, Effect of substitution by Ni in $MgAl_2O_4$ spinel for biogas dry reforming, *International Journal of Hydrogen Energy*, 2017, **42**, 24159-24168, doi: 10.1016/j.ijhydene.2017.07.222.
[30] S. Li, Q. Hao, R. Zhao, D. Liu, H. Duan, B. Dou, Highly efficient catalytic removal of ethyl acetate over Ce/Zr promoted copper/ZSM-5 catalysts, *Chemical Engineering Journal*, 2016, **285**, 536-543, doi: 10.1016/j.cej.2015.09.097.
[31] J. L. Ewbank, L. Kovarik, F. Z. Diallo, C. Sievers, Effect of metal-support interactions in Ni/Al_2O_3 catalysts with low metal loading for methane dry reforming, *Applied Catalysis A: General*, 2015, **494**, 57-67, doi: 10.1016/j.apcata.2015.01.029.
[32] D. Pan, F. Su, H. Liu, Y. Ma, R. Das, Q. Hu, C. Liu, Z. Guo, The properties and preparation methods of different boron nitride nanostructures and applications of related nanocomposites, *The Chemical Record*, 2020, **20**, 1314-1337, doi: 10.1002/tcr.202000079.
[33] Z.-Y. Tian, P. H. Tchoua Ngamou, V. Vannier, K. Kohse-Höinghaus, N. Bahlawane, Catalytic oxidation of VOCs over mixed Co-Mn oxides, *Applied Catalysis B: Environmental*, 2012, **117-118**, 125-134, doi: 10.1016/j.apcatb.2012.01.013.
[34] J. T. Bhanushali, D. Prasad, K. N. Patil, G. V. R. Babu, I. Kainthla, K. S. R. Rao, A. H. Jadhav, B. M. Nagaraja, *New Journal of Chemistry*, 2019, **43**, 11968-11983, doi: 10.1039/c9nj03067k.
[35] O. B. Ayodele, R. Cai, J. Wang, Y. Ziouani, Z. Liang, M. C. Spadaro, K. Kovnir, J. Arbiol, J. Akola, R. E. Palmer, Y. V. Kolen'ko, Synergistic computational-experimental discovery of highly selective PtCu nanocluster catalysts for acetylene semihydrogenation, *ACS Catalysis*, 2020, **10**, 451-457, doi: 10.1021/acscatal.9b03539.
[36] M. Radlik, M. Adamowska-Teyssier, A. Krztoń, K. Kozieł, W. Krajewski, W. Turek, P. da Costa, Dry reforming of methane over Ni/Ce0.62Zr0.38O2 catalysts: effect of Ni loading on the catalytic activity and on H_2/CO production, *Comptes Rendus Chimie*, 2015, **18**, 1242-1249, doi: 10.1016/j.crci.2015.03.008.
[37] C. He, J. Cheng, X. Zhang, M. Douthwaite, S. Pattisson, Z. Hao, Recent advances in the catalytic oxidation of volatile organic compounds: a review based on pollutant sorts and sources, *Chemical Reviews*, 2019, **119**, 4471-4568, doi: 10.1021/acs.chemrev.8b00408.
[38] L. Han, S. Cai, M. Gao, J.-Y. Hasegawa, P. Wang, J. Zhang, L. Shi, D. Zhang, Selective catalytic reduction of NOx with NH3 by using novel catalysts: state of the art and future prospects, *Chemical Reviews*, 2019, **119**, 10916-10976, doi: 10.1021/acs.chemrev.9b00202.
[39] J. M. Lavoie, Review on dry reforming of methane, a potentially more environmentally-friendly approach to the increasing natural gas exploitation, *Frontiers in chemistry*, 2014, **2**, 103389, doi: 10.3389/fchem.2014.00081.
[40] X. Pan, F. Jiao, D. Miao, X. Bao, Oxide-zeolite-based composite catalyst concept that enables syngas chemistry beyond Fischer-Tropsch synthesis, *Chemical Reviews*, 2021, **121**, 6588-6609, doi: 10.1021/acs.chemrev.0c01012.
[41] R. Dardouri, R. M. Navarro Yerga, N. Mota, B. Albela, L. Bonneviot, M. S. Zina, Lower methane combustion temperature on palladium nanoparticles anchored on TiO_x subnano-islets in stellate mesoporous silica nanospheres, *New Journal of Chemistry*, 2020, **44**, 906-919, doi: 10.1039/c9nj04554f.
[42] T. W. van Deelen, H. Yoshida, R. Oord, J. Zečević, B. M. Weckhuysen, K. P. de Jong, Cobalt nanocrystals on carbon nanotubes in the Fischer-Tropsch synthesis: impact of support oxidation, *Applied Catalysis A: General*, 2020, **593**, 117441, doi: 10.1016/j.apcata.2020.117441.
[43] X. Li, Y. Chen, M. U. Nisa, Z. Li, Combating poison with poison—Irreducible Co2SiO4 as a promoter to modify Co-based catalysts in Fischer-Tropsch synthesis, *Applied Catalysis B: Environmental*, 2020, **267**, 118377, doi: 10.1016/j.apcatb.2019.118377.
[44] Y. Zhang, M. Qing, H. Wang, X.-W. Liu, S. Liu, H. Wan, L. Li, X. Gao, Y. Yang, X.-D. Wen, Y.-W. Li, Comprehensive understanding of SiO_2-promoted Fe Fischer-Tropsch synthesis catalysts: Fe-SiO_2 interaction and beyond, *Catalysis Today*, 2021, **368**, 96-105, doi: 10.1016/j.cattod.2020.02.026.
[45] F. Anaya, D. E. Resasco, Enhanced Fischer-Tropsch synthesis rates by the combined presence of aqueous and organic media in biphasic systems, *ACS Catalysis*, 2020, **10**, 4433-4443, doi: 10.1021/acscatal.9b04369.
[46] M. C. Ribeiro, M. K. Gnanamani, R. Garcia, G. Jacobs, R. C. Rabelo-Neto, F. B. Noronha, I. F. Gomes, B. H. Davis, Tailoring the product selectivity of Co/SiO_2 Fischer-Tropsch synthesis catalysts by lanthanide doping, *Catalysis Today*, 2020, **343**, 80-90, doi: 10.1016/j.cattod.2018.10.064.
[47] N. E. Tsakoumis, E. Patanou, S. Lögdberg, R. E. Johnsen, R. Myrstad, W. van Beek, E. Rytter, E. A. Blekkan, Structure-performance relationships on Co-based Fischer-Tropsch synthesis catalysts: the more defect-free, the better, *ACS Catalysis*, 2019, **9**, 511-520, doi: 10.1021/acscatal.8b03549.
[48] M. A. Ocsachoque, A. Leguizamón, S. D. V. María, M. G. Gónzalez, Effect of Rh Addition to Ni/MgO-Al_2O_3 Catalysts for Dry Reforming of Methane, *Indian Journal of Science and Technology*, 2017, **10**, 1-9, doi: 10.17485/ijst/2017/v10i12/107464.
[49] A. Movasati, S. M. Alavi, G. Mazloom, Dry reforming of

methane over CeO_2-$ZnAl_2O_4$ supported Ni and Ni-Co nano-catalysts, *Fuel*, 2019, **236**, 1254-1262, doi: 10.1016/j.fuel.2018.09.069.
[50] C. Crisafulli, S. Scirè, S. Minicò, L. Solarino, Ni-Ru bimetallic catalysts for the CO_2 reforming of methane, *Applied Catalysis A: General*, 2002, **225**, 1-9, doi: 10.1016/s0926-860x(01)00585-3.
[52] Y. Turap, I. Wang, T. Fu, Y. Wu, Y. Wang, W. Wang, Co-Ni alloy supported on CeO_2 as a bimetallic catalyst for dry reforming of methane, *International Journal of Hydrogen Energy*, 2020, **45**, 6538-6548, doi: 10.1016/j.ijhydene.2019.12.223.
[53] S. Ji, Y. Qu, T. Wang, Y. Chen, G. Wang, X. Li, J. Dong, Q. Chen, W. Zhang, Z. Zhang, S. Liang, R. Yu, Y. Wang, D. Wang, Y. Li, *Angewandte Chemie International Edition*, 2020, **59**, 10651-10657, doi: 10.1002/anie.202003623.
[54] K. Liu, X. Zhao, G. Ren, T. Yang, Y. Ren, A. F. Lee, Y. Su, X. Pan, J. Zhang, Z. Chen, J. Yang, X. Liu, T. Zhou, W. Xi, J. Luo, C. Zeng, H. Matsumoto, W. Liu, Q. Jiang, K. Wilson, A. Wang, B. Qiao, W. Li, T. Zhang, Strong metal-support interaction promoted scalable production of thermally stable single-atom catalysts, *Nature Communications*, 2020, **11**, 1263, doi: 10.1038/s41467-020-14984-9.
[55] R. Xu, C. Hou, G. Xia, X. Sun, M. Li, H. Nie, D. Li, Effects of Ag promotion for Co/Al_2O_3 catalyst in Fischer-Tropsch synthesis, *Catalysis Today*, 2020, **342**, 111-114, doi: 10.1016/j.cattod.2019.04.004.
[56] S. Taghavi, A. Tavasoli, A. Asghari, M. Signoretto, Loading and promoter effects on the performance of nitrogen functionalized graphene nanosheets supported cobalt Fischer-Tropsch synthesis catalysts, *International Journal of Hydrogen Energy*, 2019, **44**, 10604-10615, doi: 10.1016/j.ijhydene.2019.03.015.
[57] Y. Wang, L. Yao, Y. Wang, S. Wang, Q. Zhao, D. Mao, C. Hu, Low-temperature catalytic CO_2 dry reforming of methane on Ni-Si/ZrO_2 catalyst, *ACS Catalysis*, 2018, **8**, 6495-6506, doi: 10.1021/acscatal.8b00584.
[58] M. Konsolakis, S. A. C. Carabineiro, G. E. Marnellos, M. F. Asad, O. S. G. P. Soares, M. F. R. Pereira, J. J. M. Órfão, J. L. Figueiredo, Volatile organic compounds abatement over copper-based catalysts: effect of support, *Inorganica Chimica Acta*, 2017, **455**, 473-482, doi: 10.1016/j.ica.2016.07.059.
[59] X. Zhang, X. Zhang, L. Song, F. Hou, Y. Yang, Y. Wang, N. Liu, Enhanced catalytic performance for CO oxidation and preferential CO oxidation over CuO/CeO2 catalysts synthesized from metal organic framework: effects of preparation methods, *International Journal of Hydrogen Energy*, 2018, **43**, 18279-18288, doi: 10.1016/j.ijhydene.2018.08.060.
[60] X. Zhang, Z. Qu, F. Yu, Y. Wang, High-temperature diffusion induced high activity of SBA-15 supported Ag particles for low temperature CO oxidation at room temperature, *Journal of Catalysis*, 2013, **297**, 264-271, doi: 10.1016/j.jcat.2012.10.019.
[61] J. Yang, J. Guo, Y. Wang, T. Wang, J. Gu, L. Peng, N. Xue, Y. Zhu, X. Guo, W. Ding, Reduction-oxidation pretreatment enhanced catalytic performance of Co_3O_4/Al_2O_3 over CO oxidation, *Applied Surface Science*, 2018, **453**, 330-335, doi: 10.1016/j.apsusc.2018.05.103.
[62] S. Carabineiro, M. Konsolakis, G. Marnellos, M. Asad, O. Soares, P. Tavares, M. Pereira, J. Órfão, J. Figueiredo, Ethyl acetate abatement on copper catalysts supported on ceria doped with rare earth oxides, *Molecules*, 2016, **21**, 644, doi: 10.3390/molecules21050644.
[63] J. I. Gutiérrez-Ortiz, B. de Rivas, R. López-Fonseca, J. R. González-Velasco, Effect of the presence of n-hexane on the catalytic combustion of chlororganics over ceria-zirconia mixed oxides, *Catalysis Today*, 2005, **107-108**, 933-941, doi: 10.1016/j.cattod.2005.07.045.
[64] J. I. Gutiérrez-Ortiz, B. de Rivas, R. López-Fonseca, J. R. González-Velasco, Catalytic purification of waste gases containing VOC mixtures with Ce/Zr solid solutions, *Applied Catalysis B: Environmental*, 2006, **65**, 191-200, doi: 10.1016/j.apcatb.2006.02.001.
[65] W. Chou, P. Wu, M. Luo, W. Li, S. Li, Effects of Al, Si, Ti, Zr promoters on catalytic performance of iron-based Fischer-Tropsch synthesis catalysts, *Catalysis Letters*, 2020, **150**, 1993-2002, doi: 10.1007/s10562-020-03104-3.
[66] Z. Zuo, S. Liu, Z. Wang, C. Liu, W. Huang, J. Huang, P. Liu, Dry reforming of methane on single-site Ni/MgO catalysts: importance of site confinement, *ACS Catalysis*, 2018, **8**, 9821-9835, doi: 10.1021/acscatal.8b02277.
[67] J. Dou, R. Zhang, X. Hao, Z. Bao, T. Wu, B. Wang, F. Yu, Sandwiched SiO_2@Ni@ZrO_2 as a coke resistant nanocatalyst for dry reforming of methane, *Applied Catalysis B: Environmental*, 2019, **254**, 612-623, doi: 10.1016/j.apcatb.2019.05.021.
[68] N. Laosiripojana, S. Assabumrungrat, Catalytic dry reforming of methane over high surface area ceria, *Applied Catalysis B: Environmental*, 2005, **60**, 107-116, doi: 10.1016/j.apcatb.2005.03.001.
[69] A. I. Tsyganok, T. Tsunoda, S. Hamakawa, K. Suzuki, K. Takehira, T. Hayakawa, Dry reforming of methane over catalysts derived from nickel-containing Mg–Al layered double hydroxides, *Journal of Catalysis*, 2003, **213**, 191-203, doi: 10.1016/S0021-9517(02)00047-7.
[70] A. Djaidja, S. Libs, A. Kiennemann, A. Barama, Characterization and activity in dry reforming of methane on NiMg/Al and Ni/MgO catalysts, *Catalysis Today*, 2006, **113**, 194-200, doi: 10.1016/j.cattod.2005.11.066.
[71] J. Guo, H. Lou, H. Zhao, D. Chai, X. Zheng, Dry reforming of methane over nickel catalysts supported on magnesium aluminate spinels, *Applied Catalysis A: General*, 2004, **273**, 75-82, doi: 10.1016/j.apcata.2004.06.014.
[72] R. O. da Fonseca, R. C. Rabelo-Neto, R. C. C. Simões, L. V. Mattos, F. B. Noronha, Pt supported on doped CeO2/Al2O3 as catalyst for dry reforming of methane, *International Journal of Hydrogen Energy*, 2020, **45**, 5182-5191, doi: 10.1016/j.ijhydene.2019.09.207.
[73] Q. Xu, Z. Fang, Y. Chen, Y. Guo, Y. Guo, L. Wang, Y. Wang, J. Zhang, W. Zhan, Titania-samarium-Manganese composite oxide for the low-temperature selective catalytic reduction of NO with NH_3, *Environmental Science & Technology*, 2020, **54**, 2530-2538, doi: 10.1021/acs.est.9b06701.

[74] Q. Chen, G. Liu, S. Ding, M. Chanmiya Sheikh, D. Long, Y. Yoneyama, N. Tsubaki, Design of ultra-active iron-based Fischer-Tropsch synthesis catalysts over spherical mesoporous carbon with developed porosity, *Chemical Engineering Journal*, 2018, **334**, 714-724, doi: 10.1016/j.cej.2017.10.093.
[75] R. Velinova, S. Todorova, B. Drenchev, G. Ivanov, M. Shipochka, P. Markov, D. Nihtianova, D. Kovacheva, A. V. Larin, A. Naydenov, Complex study of the activity, stability and sulfur resistance of Pd/La_2O_3-CeO_2-Al_2O_3 system as monolithic catalyst for abatement of methane, *Chemical Engineering Journal*, 2019, **368**, 865-876, doi: 10.1016/j.cej.2019.03.017.
[76] S. Zhang, Y. Zhao, Z. Wang, J. Zhang, L. Wang, C. Zheng, Integrated removal of NO and mercury from coal combustion flue gas using Manganese oxides supported on TiO_2, *Journal of Environmental Sciences*, 2017, **53**, 141-150, doi: 10.1016/j.jes.2015.10.038.
[77] D. P. Debecker, K. Bouchmella, R. Delaigle, P. Eloy, C. Poleunis, P. Bertrand, E. M. Gaigneaux, P. H. Mutin, One-step non-hydrolytic Sol-gel preparation of efficient V_2O_5-TiO_2 catalysts for VOC total oxidation, *Applied Catalysis B: Environmental*, 2010, **94**, 38-45, doi: 10.1016/j.apcatb.2009.10.018.
[78] B. de Rivas, R. López-Fonseca, C. Jiménez-González, J. I. Gutiérrez-Ortiz, Synthesis, characterisation and catalytic performance of nanocrystalline Co_3O_4 for gas-phase chlorinated VOC abatement, *Journal of Catalysis*, 2011, **281**, 88-97, doi: 10.1016/j.jcat.2011.04.005
[79] S. Adjimi, N. Sergent, J.-C. Roux, F. Delpech, M. Pera-Titus, K. Chhor, A. Kanaev, P.-X. Thivel, Photocatalytic paper based on Sol-gel titania nanoparticles immobilized on porous silica for VOC abatement, *Applied Catalysis B: Environmental*, 2014, **154-155**, 123-133, doi: 10.1016/j.apcatb.2014.02.011.
[80] L. Cheng, Z. Liu, S. Yuan, M. Wei, X. Hu, B. Zhang, Y. Jiang, Sol-gel citrate procedure to synthesize Ag/Co3O4 catalysts with enhanced activity for propane catalytic combustion, *Chemical Papers*, 2020, **74**, 1449-1457, doi: 10.1007/s11696-019-00994-5.
[81] Z. Cai, Q. Yao, X. Chen, X. Wang, Nanomaterials with different dimensions for electrocatalysis, *Novel Nanomaterials for Biomedical, Environmental and Energy Applications*, Elsevier, 2019, 435-464, doi: 10.1016/B978-0-12-814497-8.00014-X.
[82] R. Dorey, Routes to thick films. *Ceramic Thick Films for MEMS and Microdevices*. Amsterdam: Elsevier, 2012, 35-61, doi: 10.1016/b978-1-4377-7817-5.00002-x.
[83] Y. Wang, S. Kazumi, W. Gao, X. Gao, H. Li, X. Guo, Y. Yoneyama, G. Yang, N. Tsubaki, *Applied Catalysis B: Environmental*, 2020, **269**, 118792, doi: 10.1016/j.apcatb.2020.118792.
[84] P. Topka, M. Dvořáková, P. Kšírová, R. Perekrestov, M. Čada, J. Balabánová, M. Koštejn, K. Jirátová, F. Kovanda, Structured cobalt oxide catalysts for VOC abatement: the effect of preparation method, *Environmental Science and Pollution Research*, 2020, **27**, 7608-7617, doi: 10.1007/s11356-019-06974-2.
[85] Z.-Y. Tian, N. Bahlawane, V. Vannier, K. Kohse-Höinghaus, Structure sensitivity of propene oxidation over Co-Mn spinels, *Proceedings of the Combustion Institute*, 2013, **34**, 2261-2268, doi: 10.1016/j.proci.2012.06.182.
[86] A. El Kasmi, M. Waqas, P. Mountapmbeme Koutou, Z. Tian, Cu-promoted cobalt oxide film catalyst for efficient gas emissions abatement, *Journal of Thermal Science*, 2019, **28**, 225-231, doi: 10.1007/s11630-019-1093-9.
[87] P. M. Kouotou, Z.-Y. Tian, U. Mundloch, N. Bahlawane, K. Kohse-Höinghaus, Controlled synthesis of Co_3O_4 spinel with $Co(acac)_3$ as precursor, *RSC Advances*, 2012, **2**, 10809, doi: 10.1039/c2ra21277c.
[88] P. M. Kouotou, Z.-Y. Tian, Controlled synthesis of α-Fe_2O_3@Fe_3O_4 composite catalysts for exhaust gas purification, *Proceedings of the Combustion Institute*, 2019, **37**, 5445-5453, doi: 10.1016/j.proci.2018.05.172.
[89] A. El Kasmi, Z.-Y. Tian, H. Vieker, A. Beyer, T. Chafik, Innovative CVD synthesis of Cu_2O catalysts for CO oxidation, *Applied Catalysis B: Environmental*, 2016, **186**, 10-18, doi: 10.1016/j.apcatb.2015.12.034.
[90] Z.-Y. Tian, P. Mountapmbeme Kouotou, N. Bahlawane, P. H. Tchoua Ngamou, Synthesis of the catalytically active Mn3O4 spinel and its thermal properties, *The Journal of Physical Chemistry C*, 2013, **117**, 6218-6224, doi: 10.1021/jp312444s.
[91] M. Waqas, P. Mountapmbeme Kouotou, A. El Kasmi, Y. Wang, Z.-Y. Tian, Role of copper grid mesh in the catalytic oxidation of CO over one-step synthesized Cu-Fe-Co ternary oxides thin film, *Chinese Chemical Letters*, 2020, **31**, 1201-1206, doi: 10.1016/j.cclet.2019.06.042.
[92] I. V. Tudose, F. Comanescu, P. Pascariu, S. Bucur, L. Rusen, F. Iacomi, E. Koudoumas, M. P. Suchea, Chemical and physical methods for multifunctional nanostructured interface fabrication, *Functional Nanostructured Interfaces for Environmental and Biomedical Applications*, 2019, 15-26, doi: 10.1016/B978-0-12-814401-5.00002-5.
[93] M. V. Atamanov, M. M. Khrushchov, E. A. Marchenko, N. V. Shevchenko, I. S. Levin, M. I. Petrzhik, V. I. Miroshnichenko, M. D. Relianu, Chromium-nanodiamond coatings obtained by magnetron sputtering and their tribological properties, *Journal of Physics: Conference Series*, 2017, **872**, 012034, doi: 10.1088/1742-6596/872/1/012034.
[94] C. L. Liao, Y. H. Lee, S. T. Chang, K. Z. Fung, Structural characterization and electrochemical properties of RF-sputtered nanocrystalline Co_3O_4 thin-film anode, *Journal of Power Sources*, 2006, **158**, 1379-1385, doi: 10.1016/j.jpowsour.2005.10.014.
[95] J. S. McCloy, W. Jiang, W. Bennett, M. Engelhard, J. Lindemuth, N. Parmar, G. J. Exarhos, Electrical and magnetic properties modification in heavy ion irradiated nanograin $Ni_xCo_{(3-x)}O_4$ films, *The Journal of Physical Chemistry C*, 2015, **119**, 22465-22476, doi: 10.1021/acs.jpcc.5b06406.
[96] E. C. Lovell, H. Großman, J. Horlyck, J. Scott, L. Mädler, R. Amal, Asymmetrical double flame spray pyrolysis-designed SiO_2/$Ce_{0.7}Zr_{0.3}O_2$ for the dry reforming of methane, *ACS Applied Materials & Interfaces*, 2019, **11**, 25766-25777, doi: 10.1021/acsami.9b02572.
[97] X. Chen, Z. Xu, F. Yang, H. Zhao, Flame spray pyrolysis synthesized CuO-TiO_2 nanoparticles for catalytic combustion of

lean CO, *Proceedings of the Combustion Institute*, 2019, **37**, 5499-5506, doi: 10.1016/j.proci.2018.05.102.
[98] S. Liu, H. Zhang, M. T. Swihart, Spray pyrolysis synthesis of ZnS nanoparticles from a single-source precursor, *Nanotechnology*, 2009, **20**, 235603, doi: 10.1088/0957-4484/20/23/235603.
[99] S. Somboonthanakij, O. Mekasuwandumrong, J. Panpranot, T. Nimmanwudtipong, R. Strobel, S. E. Pratsinis, P. Praserthdam, Characteristics and catalytic properties of Pd/SiO_2 synthesized by one-step flame spray pyrolysis in liquid-phase hydrogenation of 1-heptyne, *Catalysis Letters*, 2007, **119**, 346-352, doi: 10.1007/s10562-007-9242-2.
[100] R. Zhang, W. Y. Teoh, R. Amal, B. Chen, S. Kaliaguine, Catalytic reduction of NO by CO over $Cu/Ce_xZr_{1-x}O_2$ prepared by flame synthesis, *Journal of Catalysis*, 2010, **272**, 210-219, doi: 10.1016/j.jcat.2010.04.001.
[101] L. Mädler, W. J. Stark, S. E. Pratsinis, Flame-made ceria nanoparticles, *Journal of Materials Research*, 2002, **17**, 1356-1362, doi: 10.1557/jmr.2002.0202.
[102] J. Cooper, Thesis and dissertations, *Canadian Journal of Occupational Therapy*, 1985, **52**, 36-36, doi: 10.1177/000841748505200114.
[103] N. Patel, A. Miotello, V. Bello, Pulsed Laser Deposition of Co-nanoparticles embedded on B-thin film: a very efficient catalyst produced in a single-step process, *Applied Catalysis B: Environmental*, 2011, **103**, 31-38, doi: 10.1016/j.apcatb.2011.01.005.
[104] C. Araújo, B. G. Almeida, M. Aguiar, J. A. Mendes, Structural and magnetic properties of $CoFe_2O_4$ thin films deposited by laser ablation on Si (001) substrates, *Vacuum*, 2008, **82**, 1437-1440, doi: 10.1016/j.vacuum.2008.03.014.
[105] D. W. Shin, J.-W. Choi, Y. S. Cho, S.-J. Yoon, Phase evolution and Sn-substitution in LiMn2O4 thin films prepared by pulsed laser deposition, *Journal of Electroceramics*, 2009, **23**, 200-205, doi: 10.1007/s10832-007-9378-x.
[106] J. Cheung, K. Bogle, X. Cheng, J. Sullaphen, C.-Y. Kuo, Y.-J. Chen, H.-J. Lin, C.-T. Chen, J.-C. Yang, Y.-H. Chu, N. Valanoor, Phase evolution of magnetite nanocrystals on oxide supports via template-free bismuth ferrite precursor approach, *Journal of Applied Physics*, 2012, **112**, 104321, doi: 10.1063/1.4766748.
[107] F. Ren, R. Xin, X. Ge, Y. Leng, Characterization and structural analysis of zinc-substituted hydroxyapatites, *Acta Biomaterialia*, 2009, **5**, 3141-3149, doi: 10.1016/j.actbio.2009.04.014.
[108] J. Wang, S. Huang, S. Howard, B. W. Muir, H. Wang, D. F. Kennedy, X. Ma, Elucidating surface and bulk phase transformation in Fischer-Tropsch synthesis catalysts and their influences on catalytic performance, *ACS Catalysis*, 2019, **9**, 7976-7983, doi: 10.1021/acscatal.9b01104.
[109] H. Yoshida, S. Mizuba, A. Yamamoto, Preparation of sodium hexatitanate photocatalysts by a flux method for photocatalytic steam reforming of methane, *Catalysis Today*, 2019, **334**, 30-36, doi: 10.1016/j.cattod.2019.02.055.
[110] Y. Chen, Z. Huang, M. Zhou, Z. Ma, J. Chen, X. Tang, Single silver adatoms on nanostructured Manganese oxide surfaces: boosting oxygen activation for benzene abatement, *Environmental Science & Technology*, 2017, **51**, 2304-2311, doi: 10.1021/acs.est.6b04340.
[111] M. Zhou, M. Yang, X. Yang, X. Zhao, L. Sun, W. Deng, A. Wang, J. Li, T. Zhang, On the mechanism of H_2 activation over single-atom catalyst: an understanding of Pt1/WO in the hydrogenolysis reaction, *Chinese Journal of Catalysis*, 2020, **41**, 524-532, doi: 10.1016/s1872-2067(19)63517-5.
[112] P. Maitarad, J. Han, D. Zhang, L. Shi, S. Namuangruk, T. Rungrotmongkol, Structure-activity relationships of NiO on CeO_2 nanorods for the selective catalytic reduction of NO with NH3: experimental and DFT studies, *The Journal of Physical Chemistry C*, 2014, **118**, 9612-9620, doi: 10.1021/jp5024845.
[113] M. Konsolakis, S. A. C. Carabineiro, P. B. Tavares, J. L. Figueiredo, Redox properties and VOC oxidation activity of Cu catalysts supported on $Ce_{1-x}Sm_xO_\delta$ mixed oxides, *Journal of Hazardous Materials*, 2013, **261**, 512-521, doi: 10.1016/j.jhazmat.2013.08.016.
[114] L. Lamaita, M. A. Peluso, J. E. Sambeth, H. J. Thomas, Synthesis and characterization of Manganese oxides employed in VOCs abatement, *Applied Catalysis B: Environmental*, 2005, **61**, 114-119, doi: 10.1016/j.apcatb.2005.03.014.
[115] M. Boudjeloud, A. Boulahouache, C. Rabia, N. Salhi, La-doped supported Ni catalysts for steam reforming of methane, *International Journal of Hydrogen Energy*, 2019, **44**, 9906-9913, doi: 10.1016/j.ijhydene.2019.01.140.
[116] P. Xie, T. Pu, A. Nie, S. Hwang, S. C. Purdy, W. Yu, D. Su, J. T. Miller, C. Wang, Nanoceria-supported single-atom platinum catalysts for direct methane conversion, *ACS Catalysis*, 2018, **8**, 4044-4048, doi: 10.1021/acscatal.8b00004.
[117] S.-B. Fan, G.-F. Pan, J. Liang, Z.-Y. Tian, Tailored synthesis of CoO_X thin films for catalytic application, *RSC Advances*, 2015, **5**, 97272-97278, doi: 10.1039/c5ra20013j.
[118] K. de Oliveira Rocha, C. M. P. Marques, J. M. C. Bueno, Effect of Au doping of Ni/Al_2O_3 catalysts used in steam reforming of methane: mechanism, apparent activation energy, and compensation effect, *Chemical Engineering Science*, 2019, **207**, 844-852, doi: 10.1016/j.ces.2019.06.049.
[119] H. Qiu, J. Ran, J. Niu, F. Guo, Z. Ou, Effect of different doping ratios of Cu on the carbon formation and the elimination on Ni (111) surface: a DFT study, *Molecular Catalysis*, 2021, **502**, 111360, doi: 10.1016/j.mcat.2020.111360.
[120] P. Maitarad, A. Junkaew, V. Promarak, L. Shi, S. Namuangruk, Complete catalytic cycle of NO decomposition on a silicon-doped nitrogen-coordinated graphene: Mechanistic insight from a DFT study, *Applied Surface Science*, 2020, **508**, 145255, doi: 10.1016/j.apsusc.2020.145255.
[121] G. X. Pei, X. Y. Liu, X. Yang, L. Zhang, A. Wang, L. Li, H. Wang, X. Wang, T. Zhang, Performance of Cu-alloyed Pd single-atom catalyst for semihydrogenation of acetylene under simulated front-end conditions, *ACS Catalysis*, 2017, **7**, 1491-1500, doi: 10.1021/acscatal.6b03293.
[122] H. C. Genuino, S. Dharmarathna, E. C. Njagi, M. C. Mei, S. L. Suib, Gas-phase total oxidation of benzene, toluene,

ethylbenzene, and xylenes using shape-selective Manganese oxide and copper Manganese oxide catalysts, *The Journal of Physical Chemistry C*, 2012, **116**, 12066-12078, doi: 10.1021/jp301342f.
[123] Z. Zhang, Z. Jiang, W. Shangguan, Low-temperature catalysis for VOCs removal in technology and application: a state-of-the-art review, *Catalysis Today*, 2016, **264**, 270-278, doi: 10.1016/j.cattod.2015.10.040.
[124] M. Konsolakis, S. A. C. Carabineiro, G. E. Marnellos, M. F. Asad, O. S. G. P. Soares, M. F. R. Pereira, J. J. M. Órfão, J. L. Figueiredo, Volatile organic compounds abatement over copper-based catalysts: effect of support, *Inorganica Chimica Acta*, 2017, **455**, 473-482, doi: 10.1016/j.ica.2016.07.059.
[125] L.-N. Wu, Z.-Y. Tian, W. Qin, Mechanism of CO Oxidation on Cu_2O (111) Surface: A DFT and Microkinetic Study, *International Journal of Chemical Kinetics*, 2018, **50**, 507-514, doi: 10.1002/kin.21176.
[126] V. V. Kaichev, A. Y. Gladky, I. P. Prosvirin, A. A. Saraev, M. Hävecker, A. Knop-Gericke, R. Schlögl, V. I. Bukhtiyarov, In situ XPS study of self-sustained oscillations in catalytic oxidation of propane over nickel, *Surface science*, 2013, **609**, 113-118, doi: 10.1016/j.susc.2012.11.012 Scopus.
[127] T. K. Tseng, H. Chu, The kinetics of catalytic incineration of styrene over a MnO/Fe_2O_3 catalyst, *Science of the Total Environment*, 2001, **275**, 83-93, doi: 10.1016/s0048-9697(00)00856-1.
[128] J. C.-S. Wu, Z.-A. Lin, F.-M. Tsai, J.-W. Pan, Low-temperature complete oxidation of BTX on Pt/activated carbon catalysts, *Catalysis Today*, 2000, **63**, 419-426, doi: 10.1016/s0920-5861(00)00487-9.
[129] L. F. Liotta, Catalytic oxidation of volatile organic compounds on supported noble metals, *Applied Catalysis B: Environmental*, 2010, **100**, 403-412, doi: 10.1016/j.apcatb.2010.08.023 Scopus.
[130] A. Aranzabal, J. L. Ayastuy-Arizti, J. A. González-Marcos, J. R. González-Velasco, Kinetics of the catalytic oxidation of lean trichloroethylene in air over Pd/alumina, *Industrial & Engineering Chemistry Research*, 2003, **42**, 6007-6011, doi: 10.1021/ie030286r.
[131] C. Yang, G. Miao, Y. Pi, Q. Xia, J. Wu, Z. Li, J. Xiao, Abatement of various types of VOCs by adsorption/catalytic oxidation: a review, *Chemical Engineering Journal*, 2019, **370**, 1128-1153, doi: 10.1016/j.cej.2019.03.232.
[132] L. Wu, W. Qin, X. Hu, S. Ju, C. Dong, Y. Yang, Decomposition and reduction of N_2O on CaS (100) surface: a theoretical account, *Surface Science*, 2015, **632**, 83-87, doi: 10.1016/j.susc.2014.09.014.
[133] L. Wu, X. Hu, W. Qin, C. Dong, Y. Yang, Effect of sulfation on the surface activity of CaO for N_2O decomposition, *Applied Surface Science*, 2015, **357**, 951-960, doi: 10.1016/j.apsusc.2015.09.006.
[134] L. Wu, X. Hu, W. Qin, P. Gao, C. Dong, Y. Yang, Effect of CaO on the selectivity of N_2O decomposition products: a combined experimental and DFT study, *Surface Science*, 2016, **651**, 128-136, doi: 10.1016/j.susc.2016.04.004.
[135] L. Wu, W. Qin, X. Hu, C. Dong, Y. Yang, Mechanism study on the influence of in situ SO removal on N_2O emission in CFB boiler, *Applied Surface Science*, 2015, **333**, 194-200, doi: 10.1016/j.apsusc.2015.01.229.
[136] P. Devaraji, W.-K. Jo, Noble metal free Fe and Cr dual-doped nanocrystalline titania ($Ti_{1-x-y}M_{x+y}O_2$) for high selective photocatalytic conversion of benzene to phenol at ambient temperature, *Applied Catalysis A: General*, 2018, **565**, 1-12, doi: 10.1016/j.apcata.2018.07.035
[137] G. Li, B. Wang, Z. Wang, Z. Li, Q. Sun, W. Q. Xu, Y. Li, Reaction mechanism of low-temperature selective catalytic reduction of NO_x over Fe-Mn oxides supported on fly-ash-derived SBA-15 molecular sieves: structure-activity relationships and in situ DRIFT analysis, *The Journal of Physical Chemistry C*, 2018, **122**, 20210-20231, doi: 10.1021/acs.jpcc.8b03135.
[138] K. Li, C. Pei, X. Li, S. Chen, X. Zhang, R. Liu, J. Gong, Dry reforming of methane over $La_2O_2CO_3$-modified Ni/Al_2O_3 catalysts with moderate metal support interaction, *Applied Catalysis B: Environmental*, 2020, **264**, 118448, doi: 10.1016/j.apcatb.2019.118448.
[139] B. Shi, Y. Liao, Z. J. Callihan, B. T. Shoopman, M. Luo, Carbon-Carbon bond formation during Fe catalyzed Fischer-Tropsch synthesis, *Applied Catalysis A: General*, 2020, **602**, 117607, doi: 10.1016/j.apcata.2020.117607.
[140] M. F. Arshad, A. El Kasmi, M. Waqas, Z.-Y. Tian, Insight into one-step synthesis of active amorphous La-Co thin films for catalytic oxidation of CO, *Applications in Energy and Combustion Science*, 2021, **5**, 100021, doi: 10.1016/j.jaecs.2020.100021.
[141] J. Li, H. Wan, H. Lv, G. Guan, Activity of Cu-Co mixed oxides monolithic catalysts supported on TiO_2 for catalytic combustion of methyl acetate, *World Automation Congress*, 2012, 1-4.
[142] M. S. L. Aparicio, I. D. Lick, Total oxidation of propane and naphthalene from emission sources with supported cobalt catalysts, Reaction Kinetics, *Mechanisms and Catalysis*, 2016, **119**, 469-479, doi: 10.1007/s11144-016-1052-3.
[143] O. U. Osazuwa, C. K. Cheng, Catalytic conversion of methane and carbon dioxide (greenhouse gases) into syngas over samarium-cobalt-trioxides perovskite catalyst, *Journal of Cleaner Production*, 2017, **148**, 202-211, doi: 10.1016/j.jclepro.2017.01.177.
[144] Z.-Y. Tian, P. H. Tchoua Ngamou, V. Vannier, K. Kohse-Höinghaus, N. Bahlawane, Catalytic oxidation of VOCs over mixed Co-Mn oxides, *Applied Catalysis B: Environmental*, 2012, **117-118**, 125-134, doi: 10.1016/j.apcatb.2012.01.013.
[145] J. Cheng, Q. Ye, C. Li, S. Cheng, T. Kang, H. Dai, Ceria-modified Al-Mn-pillared clay catalysts for the selective catalytic reduction of NO with NH3 at low temperatures, *Asia-Pacific Journal of Chemical Engineering*, 2020, **15**, e2439, doi: 10.1002/apj.2439.
[146] L. Meng, H. Zhao, Low-temperature complete removal of toluene over highly active nanoparticles $CuO-TiO_2$ synthesized via flame spray pyrolysis, *Applied Catalysis B: Environmental*, 2020, **264**, 118427, doi: 10.1016/j.apcatb.2019.118427.

[147] I. Popescu, N. Tanchoux, D. Tichit, I.-C. Marcu, I. C. G. France, Effect of the support on the catalytic activity of copper oxide in methane combustion, *National Research and Development Institute for Industrial Ecology*, 2018, doi: 10.21698/simi.2018.ab05.
[148] D. Yu, Z. Tian, M. Waqas, Z. Jin, A. E. Kasmi, D. Tian, P. M. Kouotou, Toluene abatement by non-thermal plasma coupled with thin film of Cu-Co binary oxide coated on stainless steel mesh, *ES Energy & Environment*, 2019, **5**, 75-84, doi: 10.30919/esee8c301.
[149] C. A. Chagas, F. S. Toniolo, R. N. S. H. Magalhães, M. Schmal, Alumina-supported $LaCoO_3$ perovskite for selective CO oxidation (SELOX), *International Journal of Hydrogen Energy*, 2012, **37**, 5022-5031, doi: 10.1016/j.ijhydene.2011.12.052.
[150] B. Seyfi, M. Baghalha, H. Kazemian, Modified LaCoO3 nano-perovskite catalysts for the environmental application of automotive CO oxidation, *Chemical Engineering Journal*, 2009, **148**, 306-311, doi: 10.1016/j.cej.2008.08.041.
[151] R. Beauchet, J. Mijoin, P. Magnoux, Improved catalytic oxidation of cumene by formation of catalytically active species during reaction over NaX zeolite, *Applied Catalysis B: Environmental*, 2009, **88**, 106-112, doi: 10.1016/j.apcatb.2008.09.014.
[152] R. Beauchet, P. Magnoux, J. Mijoin, Catalytic oxidation of volatile organic compounds (VOCs) mixture (isopropanol/o-xylene) on zeolite catalysts, *Catalysis Today*, 2007, **124**, 118-123, doi: 10.1016/j.cattod.2007.03.030.
[153] Y. Li, J. N. Armor, Catalytic combustion of methane over palladium exchanged zeolites, *Applied Catalysis B: Environmental*, 1994, **3**, 275-282, doi: 10.1016/0926-3373(94)0006z-h.
[154] M. Guo, P. Zhao, Q. Liu, C. Liu, J. Han, N. Ji, C. Song, D. Ma, X. Lu, X. Liang, Z. Li, Improved low-temperature activity and H_2O resistance of Fe-doped Mn–Eu catalysts for NO removal by NH_3–SCR, *ChemCatChem*, 2019, **11**, 4954-4965, doi: 10.1002/cctc.201900979.
[155] H. Jiang, Y. Wang, J. Zhou, Y. Chen, M. Zhang, Morphology control of Manganese-based catalysts for low-temperature selective catalytic reduction of NO_x, *Materials Letters*, 2018, **233**, 250-253, doi: 10.1016/j.matlet.2018.09.004.
[156] C. Fan, Z. Chen, L. Pang, S. Ming, C. Dong, K. Brou Albert, P. Liu, J. Wang, D. Zhu, H. Chen, T. Li, Steam and alkali resistant Cu-SSZ-13 catalyst for the selective catalytic reduction of NO_x in diesel exhaust, *Chemical Engineering Journal*, 2018, **334**, 344-354, doi: 10.1016/j.cej.2017.09.181.
[157] T. Li, W. Sun, Z. Zhou, T. Xie, L. Cao, J. Yang, Di-metal-doped sulfur resisting perovskite catalysts for highly efficient H2-SCR of NO, *Environmental Science and Pollution Research*, 2018, **25**, 25504-25514, doi: 10.1007/s11356-018-2608-8.
[158] A. Yamamoto, K. Teramura, S. Hosokawa, T. Tanaka, Effects of SO_2 on selective catalytic reduction of NO with NH_3 over a TiO_2 photocatalyst, *Science and Technology of Advanced Materials*, 2015, **16**, 024901, doi: 10.1088/1468-6996/16/2/024901.
[159] Y. Liu, Z. Li, Q. Yu, Y. Chen, Z. Chai, G. Zhao, S. Liu, W.-C. Cheong, Y. Pan, Q. Zhang, L. Gu, L. Zheng, Y. Wang, Y. Lu, D. Wang, C. Chen, Q. Peng, Y. Liu, L. Liu, J. Chen, Y. Li, A general strategy for fabricating isolated single metal atomic site catalysts in Y zeolite, *Journal of the American Chemical Society*, 2019, **141**, 9305-9311, doi: 10.1021/jacs.9b02936.
[160] P. Michorczyk, J. Ogonowski, P. Kuśtrowski, L. Chmielarz, Chromium oxide supported on MCM-41 as a highly active and selective catalyst for dehydrogenation of propane with CO_2, *Applied Catalysis A: General*, 2008, **349**, 62-69, doi: 10.1016/j.apcata.2008.07.008.
[161] B. Zheng, W. Hua, Y. Yue, Z. Gao, Dehydrogenation of propane to propene over different polymorphs of gallium oxide, *Journal of Catalysis*, 2005, **232**, 143-151, doi: 10.1016/j.jcat.2005.03.001.
[162] B. Xu, B. Zheng, W. Hua, Y. Yue, Z. Gao, Support effect in dehydrogenation of propane in the presence of CO_2 over supported gallium oxide catalysts, *Journal of Catalysis*, 2006, **239**, 470-477, doi: 10.1016/j.jcat.2006.02.017.
[163] L. Liu, H. Li, Y. Zhang, Mesoporous silica-supported chromium catalyst: characterization and excellent performance in dehydrogenation of propane to propylene with carbon dioxide, *Catalysis Communications*, 2007, **8**, 565-570, doi: 10.1016/j.catcom.2006.08.005.
[164] T. Otroshchenko, G. Jiang, V. A. Kondratenko, U. Rodemerck, E. V. Kondratenko, Current status and perspectives in oxidative, non-oxidative and CO_2-mediated dehydrogenation of propane and isobutane over metal oxide catalysts, *Chemical Society Reviews*, 2021, **50**, 473-527, doi: 10.1039/d0cs01140a.
[165] C. K. Fonzeu Monguen, A. El Kasmi, M. F. Arshad, P. M. Kouotou, S. Daniel, Z.-Y. Tian, Oxidative dehydrogenation of propane into propene over chromium oxides, *Industrial & Engineering Chemistry Research*, 2022, **61**, 4546-4560, doi: 10.1021/acs.iecr.2c00813.
[166] B.-J. Xu, B. Zheng, W.-M. Hua, Y.-H. Yue, Z. Gao, High Si/Al ratio HZSM-5 supported Ga_2O_3: a highly stable catalyst for dehydrogenation of propane to propene in the presence of CO_2, *Studies in surface science and catalysis*, Elsevier, 2007, **170**, 1072-1079, doi: 10.1016/S0167-2991(07)80962-1.
[167] Y. Ren, J. Wang, W. Hua, Y. Yue, Z. Gao, E. Chemistry, Ga_2O_3/HZSM-48 for dehydrogenation of propane: Effect of acidity and pore geometry of support, *Journal of Industrial and Engineering Chemistry*, 2012, **18**, 731-736, doi: 10.1016/j.jiec.2011.11.134.
[168] J. M. Venegas, I. Hermans, The influence of reactor parameters on the boron nitride-catalyzed oxidative dehydrogenation of propane, *Organic Process Research & Development*, 2018, **22**, 1644-1652, doi: 10.1021/acs.oprd.8b00301.
[169] F. Zhang, R. Wu, Y. Yue, W. Yang, S. Gu, C. Miao, W. Hua, Z. Gao, Chromium oxide supported on ZSM-5 as a novel efficient catalyst for dehydrogenation of propane with CO_2, *Microporous and Mesoporous Materials*, 2011, **145**, 194-199, doi: 10.1016/j.micromeso.2011.05.021.
[170] P. Chaturbedy, M. Ahamed, M. Eswaramoorthy, Oxidative dehydrogenation of propane over a high surface area boron

nitride catalyst: exceptional selectivity for olefins at high conversion, *ACS Omega*, 2018, **3**, 369-374, doi: 10.1021/acsomega.7b01489.
[171] R. Wu, P. Xie, Y. Cheng, Y. Yue, S. Gu, W. Yang, C. Miao, W. Hua, Z. Gao, Hydrothermally prepared Cr_2O_3-ZrO_2 as a novel efficient catalyst for dehydrogenation of propane with CO_2, *Catalysis Communications*, 2013, **39**, 20-23, doi: 10.1016/j.catcom.2013.05.002.
[172] M. Chen, J. Xu, Y. Cao, H.-Y. He, K.-N. Fan, J.-H. Zhuang, Dehydrogenation of propane over In_2O_3-Al_2O_3 mixed oxide in the presence of carbon dioxide, *Journal of Catalysis*, 2010, **272**, 101-108, doi: 10.1016/j.jcat.2010.03.007.
[173] H. Li, Y. Yue, C. Miao, Z. Xie, W. Hua, Z. Gao, Dehydrogenation of ethylbenzene and propane over Ga_2O_3-ZrO_2 catalysts in the presence of CO_2, *Catalysis Communications*, 2007, **8**, 1317-1322, doi: 10.1016/j.catcom.2006.11.034
[174] Y. A. Agafonov, N. A. Gaidai, A. L. Lapidus, Influence of the preparation conditions for catalysts CrO_x/SiO_2 on their efficiency in propane dehydrogenation in the presence CO_2, *Russian Chemical Bulletin*, 2014, **63**, 381-388, doi: 10.1007/s11172-014-0441-x.
[175] S. Daniel, C. K. F. Monguen, A. El Kasmi, M. F. Arshad, Z.-Y. Tian, Oxidative dehydrogenation of propane to olefins promoted by Zr modified ZSM-5, *Catalysis Letters*, 2022, doi: 10.1007/s10562-022-03977-6.
[176] Z. L. Zhang, X. E. Verykios, Carbon dioxide reforming of methane to synthesis gas over supported Ni catalysts, *Catalysis Today*, 1994, **21**, 589-595, doi: 10.1016/0920-5861(94)80183-5.
[177] D. Li, R. Li, M. Lu, X. Lin, Y. Zhan, L. Jiang, Carbon dioxide reforming of methane over Ru catalysts supported on Mg-Al oxides: a highly dispersed and stable Ru/Mg(Al)O catalyst, *Applied Catalysis B: Environmental*, 2017, **200**, 566-577, doi: 10.1016/j.apcatb.2016.07.050.
[178] E. Ruckenstein, Y. H. Hu, Carbon dioxide reforming of methane over nickel/alkaline earth metal oxide catalysts, *Applied Catalysis A: General*, 1995, **133**, 149-161, doi: 10.1016/0926-860x(95)00201-4.
[179] F. A. J. Al-Doghachi, U. Rashid, Z. Zainal, M. I. Saiman, Y. H. Taufiq Yap, Influence of Ce_2O_3 and CeO_2 promoters on Pd/MgO catalysts in the dry-reforming of methane, *RSC Advances*, 2015, **5**, 81739-81752, doi: 10.1039/c5ra15825g.
[180] A. S. Al-Fatesh, Promotional effect of Gd over Ni/Y_2O_3 catalyst used in dry reforming of CH_4 for H_2 production, *International Journal of Hydrogen Energy*, 2017, **42**, 18805-18816, doi: 10.1016/j.ijhydene.2017.06.165.
[181] A. G. Bhavani, W. Y. Kim, J. S. Lee, Barium substituted lanthanum manganite perovskite for CO_2 reforming of methane, *ACS Catalysis*, 2013, **3**, 1537-1544, doi: 10.1021/cs400245m.
[182] B. Jager, Developments in Fischer-Tropsch technology, *Studies in surface science and catalysis*, Elsevier, 1998, **119**, 25-34, doi: 10.1016/S0167-2991(97)80338-2.
[183] M. E. Dry, The Fischer-Tropsch process: 1950-2000, *Catalysis Today*, 2002, **71**, 227-241, doi: 10.1016/s0920-5861(01)00453-9.
[184] H. Schulz, Short history and present trends of Fischer-Tropsch synthesis, *Applied Catalysis A: General*, 1999, **186**, 3-12, doi: 10.1016/s0926-860x(99)00160-x.
[185] V. R. R. Pendyala, G. Jacobs, H. H. Hamdeh, W. D. Shafer, D. E. Sparks, S. Hopps, B. H. Davis, Fischer-Tropsch synthesis: effect of activation gas after varying Cu promoter loading over K-promoted Fe-based catalyst, *Catalysis Letters*, 2014, **144**, 1624-1635, doi: 10.1007/s10562-014-1302-9.
[186] C.-I. Ahn, Y. M. Park, J. M. Cho, D. H. Lee, C.-H. Chung, B. G. Cho, J. W. Bae, Fischer-trospch synthesis on ordered mesoporous cobalt-based catalysts with compact multichannel fixed-bed reactor application: a review, *Catalysis Surveys from Asia*, 2016, **20**, 210-230, doi: 10.1007/s10563-016-9219-5.
[187] T. K. Das, W. Conner, G. Jacobs, J. Li, K. Chaudhari, B. H. Davis, Fischer-Tropsch synthesis: effect of water on activity and selectivity for a cobalt catalyst, *Studies in surface science and catalysis*, Elsevier, 2004, **147**, 331-336, doi: 10.1016/S0167-2991(04)80073-9.
[188] C. J. Bertole, C. A. Mims, G. Kiss, The effect of water on the cobalt-catalyzed Fischer–Tropsch synthesis, *Journal of Catalysis*, 2002, **210**, 84-96, doi: 10.1006/jcat.2002.3666.
[189] G. Jacobs; T. K. Das, J. Li, M. Luo, P. M. Patterson, B. H. Davis, Fischer-Tropsch synthesis: influence of support on the impact of co-fed water for cobalt-based catalysts, *Studies in surface science and catalysis*, Elsevier, 2007, **163**, 217-253, doi: 10.1016/s0167-2991(07)80481-2.
[190] S. Storsater, O. Borg, E. Blekkan, A. Holmen, Study of the effect of water on Fischer-Tropsch synthesis over supported cobalt catalysts, *Journal of Catalysis*, 2005, **231**, 405-419, doi: 10.1016/j.jcat.2005.01.036.
[191] V. R. R. Pendyala, G. Jacobs, J. C. Mohandas, M. Luo, H. H. Hamdeh, Y. Ji, M. C. Ribeiro, B. H. Davis, Fischer-Tropsch synthesis: effect of water over iron-based catalysts, *Catalysis Letters*, 2010, **140**, 98-105, doi: 10.1007/s10562-010-0452-7.
[192] F. Rohr, A. Holmen, K. K. Barbo, P. Warloe, E. A. Blekkan, Modified alumina supports for cobalt Fischer-Tropsch catalysts, *Studies in surface science and catalysis*, 1998, **119**, 107-112, doi: 10.1016/S0167-2991(98)80416-3.
[193] A. H. Lillebø, E. Patanou, J. Yang, E. A. Blekkan, A. Holmen, The effect of alkali and alkaline earth elements on cobalt based Fischer-Tropsch catalysts, *Catalysis Today*, 2013, **215**, 60-66, doi: 10.1016/j.cattod.2013.03.030.
[194] D. G. Miller, M. Moskovits, A study of the effects of potassium addition to supported iron catalysts in the Fischer-Tropsch reaction, *The Journal of Physical Chemistry*, 1988, **92**, 6081-6085, doi: 10.1021/j100332a047.
[195] M. Feyzi, M. Irandoust, A. A. Mirzaei, Effects of promoters and calcination conditions on the catalytic performance of iron-Manganese catalysts for Fischer-Tropsch synthesis, *Fuel Processing Technology*, 2011, **92**, 1136-1143, doi: 10.1016/j.fuproc.2011.01.010.
[196] B. Øyvind, R. Magnus, S. SØlvi, v. B. Wouter, H. Anders, Identification of cobalt species during temperature programmed reduction of Fischer-Tropsch catalysts, *Studies in surface science and catalysis*, Elsevier, 2007, **163**, 255-272, doi: 10.1016/s0167-2991(07)80482-4.

[197] S. S. Itkulova, G. D. Zakumbaeva, R. S. Arzumanova, V. A. Ovchinnikov, Production of hard hydrocarbons from synthesis-gas over co-containing supported catalysts, *Studies in surface science and catalysis*, 2007, **163**, 75-85, doi: 10.1016/s0167-2991(07)80473-3.
[198] W. Ma, E. L. Kugler, D. B. Dadyburjor, Effect of Mo loading and support type on hydrocarbons and oxygenates produced over Fe-Mo-Cu-K catalysts supported on activated carbons, *Studies in surface science and catalysis*, Elsevier, 2007, **163**, 125-140, doi: 10.1016/s0167-2991(07)80476-9.
[199] T. K. Das, G. Jacobs, P. M. Patterson, W. A. Conner, J. Li, B. H. Davis, Fischer-Tropsch synthesis: characterization and catalytic properties of rhenium promoted cobalt alumina catalysts, *Fuel*, 2003, **82**, 805-815, doi: 10.1016/s0016-2361(02)00361-7.

Author Information

Cedric Karel Fonzeu Monguen *received his Master Engineering degree in 2016 from the National Advanced Polytechnic of Maroua, University of Maroua, Cameroon. He is pursuing his PhD in power engineering and engineering thermophysics at the Institute of Engineering Thermophysics, University of Chinese Academy of Sciences. He is working under the supervision of Prof. Zhen-Yu Tian. His main areas of research interest are heterogeneous catalysis, thin films and nanotechnology, materials synthesis, and environmental chemistry.*

Samuel Daniel *received his bachelor degree in 2017 from Modibbo Adama University Yola, Nigeria. He is currently a PhD candidate in Environmental Engineering at the Institute of Engineering Thermophysics, University of Chinese Academy of Sciences, under the supervision of Prof. Zhen-Yu Tian. His research interests focus on the modification of ZSM-5 for alkane dehydrogenation and VOC oxidation.*

Dr. Dan Yu*, Director of Environmental Technology, Academy of Research/Small Domestic Application Division, Midea Group. She got her PhD in 2011 in the Institute of Chemistry, CAS, and worked as a postdoc at Tsinghua University during 2011-2015. In 2016-2021, she worked at the Institute of Engineering Thermophysics, CAS. She majors in air-space combustion and air purification in the energy and environmental field. She has been the expert reviewer of the National Natural Science Foundation of China, Annual Meeting of Engineering Thermophysics-Combustion and Journal of Combustion Science and Technology.*

Dr. Olumide Bolarinwa Ayodele *is an Associate Professor at University of Texas at San Antonio, Texas, United States. In 2015, he obtained his PhD at University of Malaya Kuala Lumpur, Malaysia. He was a research fellow at International Iberian Nanotechnology Laboratory Braga, Portugal in 2018-2020. He was a visiting scholar at University of Regina, Canada and the Institute of Engineering Thermophysics, CAS in 2020-2021. His research interests include catalytic upgrading of bio-oil via the hydrodeoxygenation process, heterogeneous catalysis, reaction kinetics, computer-aided process engineering design and simulation.*

Prof. Zhen-Yu Tian *got his PhD at the University of Science and Technology in 2008. Then he did a postdoc at CNRS in France (2008-2010) and worked at Bielefeld University as an Alexander von Humboldt Fellow and group leader (2010-2013). From August 2013, he works as a full Professor at the Institute of Engineering Thermophysics, Chinese Academy of Sciences (CAS). Tian's group mainly focuses on the combustion kinetics of engines, thin films, catalysis, environmental chemistry, microgravity combustion and physical chemistry. The current project is the kinetic study of homogeneous and heterogeneous combustion.*